

Article

Dynamics of Oxidation of Reduced Forms of CO₂ under Electrochemical and Open-Circuit Conditions on Polycrystalline Pt in H₂CO₃

Alexander V. Smolin¹, Mikhail N. Mikhailov¹, Aleksey F. Gadzaov² and Leonid M. Kustov^{1,3,4,*}

¹ N.D. Zelinsky Institute of Organic Chemistry, 47 Leninsky Prospect, 119991 Moscow, Russia; asmolin13@yandex.ru (A.V.S.); mikhail.n.mikhailov@gmail.com (M.N.M.)

² Federal State Budget Educational Institution of Higher Education, MIREA—Russian Technological University, RTU MIREA 78, Vernadskogo Ave., 119454 Moscow, Russia; gadzaov_alex@mail.ru

³ Institute of Ecotechnologies and Engineering, National University of Science and Technology MISiS, 4 Leninsky Prospect, 119991 Moscow, Russia

⁴ Chemistry Department, Moscow State University, 1 Leninskie Gory, bldg. 3, 119992 Moscow, Russia

* Correspondence: lmkustov@mail.ru; Tel.: +7-910-414-0702

Abstract: The problem of identifying correlations between catalytic and electrocatalytic processes is one of the fundamental problems of catalysis among “simple” organic substances, and the oxidation of CO and rCO₂ is of great interest, since CO and CO₂ are considered in pairs both during catalytic and electrocatalytic transformations. In the case of electrocatalysis, this analysis is important in the study of fuel cells. In this paper, we studied the correlation between the oxidation of reduced forms of CO₂ (rCO₂) under potentiodynamic-galvanostatic electrochemical and open-circuit conditions of measurements on polycrystalline (pc)Pt in H₂CO₃. Periodic oscillations are revealed at the oxidation of H_{ad} and rCO₂ on (pc)Pt. Quantum chemical calculations were carried out on the Pt₁₃ cluster in order to identify the mechanisms of the rCO₂ oxidation reaction. The correspondence in the energy parameters of the oxidation process of rCO₂ under open-circuit conditions and electrochemical conditions is shown. The preliminary analysis of the system using density functional (DFT) calculations is carried out and the most stable systems that are based on Pt₁₃ are found, namely rOH-Pt₁₃-(CO)_n, rOH-Pt₁₃-(COH) and rOH-Pt₁₃-(rCOOH). OH[•] species was chosen as the most likely candidate for the role of the oxidant for rCO₂. Preliminary calculations for the expected reactions were carried out, and the optimal PES is revealed.

Keywords: platinum; carbon dioxide; carbon monoxide; hydrogen peroxide; reduction; oxidation; electrochemical processes



Citation: Smolin, A.V.; Mikhailov, M.N.; Gadzaov, A.F.; Kustov, L.M. Dynamics of Oxidation of Reduced Forms of CO₂ under Electrochemical and Open-Circuit Conditions on Polycrystalline Pt in H₂CO₃. *Metals* **2021**, *11*, 274. <https://doi.org/10.3390/met11020274>

Academic Editor: Marco Martino

Received: 17 December 2020

Accepted: 1 February 2021

Published: 5 February 2021

Publisher's Note: MDPI stays neutral with regard to jurisdictional claims in published maps and institutional affiliations.



Copyright: © 2021 by the authors. Licensee MDPI, Basel, Switzerland. This article is an open access article distributed under the terms and conditions of the Creative Commons Attribution (CC BY) license (<https://creativecommons.org/licenses/by/4.0/>).

1. Introduction

The interest to the electrochemical transformations of CO₂ mainly originates from the identification of electrochemical conditions for CO₂ reduction in order to obtain useful products. As to the global challenges, this is related to CO₂ utilization. The catalytic reaction of reverse water gas shift—the conversion of CO₂ to CO—is well known to proceed on Pt. The main product of the electrochemical reduction of CO₂ on Pt is CO. The low solubility of CO₂ in water, significant energy costs, and low quantitative yields of products due to the hydrogen reduction reaction (HRR) are the main problems with the electrochemical conversion of CO₂ in water [1].

Among the “simple” organic substances, CO and CO₂ are of utmost interest. These substances are often considered in a pair in both the course of the catalytic and electrocatalytic transformations. In the case of the electrocatalysis, this analysis is important in the study from the point of view of effective fuel cells. There are two problems that arise when creating fuel cells that are based on organic fuel processing: poisoning of the catalyst surface with fuel chemisorption products, which leads to a decrease in the efficiency of

the fuel cell, and the fuel crossover from the anode space to the cathode of the fuel cell. The latter can lead to the polarization of the anode and a decrease in its potential and additional fuel consumption due to its interaction with the oxidizer. The performance of a hydrogen-oxygen fuel cell can significantly deteriorate as a result of the adsorption of CO, which is usually present in H₂ as an impurity. One way to reduce the poisoning of catalysts with carbon monoxide is to add small amounts of O₂ to the oxidized H₂. Therefore, investigations that are focused on the O₂ reduction reaction (ORR) and the transformation of its products, for example, H₂O₂ on the cathode in conjugated electrocatalytic reactions, are extremely important. To date, there has been extensive literature on these reactions. In the last five years, more than 1000 review articles have been published on various electrodes, in different systems, and under different conditions. Much attention continues to be paid to the Pt electrode in relation to the above reactions [2–8]. This is also important in view of the development of highly sensitive oxygen sensors.

On the other hand, the problem of identifying the correlations between catalytic and electrocatalytic processes is one of the fundamental problems of catalysis [9–13]. Previously, the problems of the theory of current transients arising upon introducing “neutral” CO-type particles into the contact with Pt-group metal electrodes were considered [10–13] on the basis of thermodynamic ideas regarding the full charge of the electrode [14,15]. These ideas were further developed while analyzing the relationship between the transients of the current (the use of potentiostatic current transients (I, t—curves) (potentiostatic chronoamperometry) is an important method in electrocatalysis, because it allows one to study, in detail, the kinetics of electrocatalytic reactions and to determine the amount of electricity during electrolysis, thereby correlating the measured I values with the chosen value of the potential in stationary conditions, electrocatalytic reactions.) and the potential in the absence of the current upon adsorption of some neutral particles [13]. Kinetics studies were carried out in relation to the oxidation reactions of “simple” organic substances containing only one carbon atom (C1) with adsorbed oxygen O_{ads} on Pt under open circuit conditions with the registration of transients of the no-current potential. CO, HCOOH [16,17], CH₃OH [18], HCHO [19], and molecules with the number of carbon atoms more than 1, i.e., homologs of aliphatic alcohols ROH [20] were chosen as substrates for oxidation. The correlation of the data that were obtained under the conditions of catalytic and electrocatalytic measurements was revealed in the calculations of the CH₃OH oxidation dynamics [21]. It was shown from the first principles that the main difference between the catalytic oxidation of methanol in the gas phase and the electrocatalytic oxidation of CH₃OH in an aqueous electrolyte was related to the difference in the nature of oxidizing particles—atomic O and OH species, respectively. In addition, molecules of diols can be formed in the aqueous medium, while they are absent in the gas-phase process.

The oscillation nature of oxidation reactions in both electrocatalytic and catalytic conditions has been found for many C1 substrates, including CO on Pt [22–26]. In the study of oxidation reactions of ROH [20] in an H₂SO₄ aqueous solution by the methods of the no-current potential transients (E_{nc},t curves) in combination with potentiodynamic pulses, the oscillations were revealed on the experimental E_{nc},t curves [27]. When comparing the analysis results of these transients that are determined by the different methods [20,27], it turned out that they are complementary to each other, and they are not contradictory and expand the understanding of the chemistry of the processes. The data that were obtained under open-circuit conditions correlated with the experimental data under electrochemical measurements for CH₃OH, with the oxidation of the latter resulting in the formation of CO₂, HCOOH, HCHO [28], and C₂H₅OH, with the main oxidation products being CH₃COOH or CH₃CHO [29], as well as small amounts of CO₂.

A new method for removing dissolved gases from water has been proposed in [30]. It is based on a “helium washing” procedure. For electrocatalytic processes, this technique is useful for obtaining ultra-low concentrations of dissolved O₂ in H₂O. This makes it possible to perform electrochemical measurements on a smooth Pt electrode under both electrochemical and open circuit conditions, while minimizing the contribution of the conjugated

ORR. This allows for one to study, in detail, the oxidation of adsorbates on electrodes with dissolved O_2 under conditions of long-term measurements. Therefore, the use of such a technique can create favorable conditions for the development of electrochemical sensors for the ultra-low O_2 content in the volume of the solution. The oxidation reaction of rCO_2 on a smooth polycrystalline (pc) Pt electrode in a saturated solution of carbonic acid under open-circuit and electrochemical conditions was chosen as a model system for studying the oxidation of adsorbates under the conditions of ultra-low dissolved O_2 concentrations.

It is known that, when CO_2 is reduced in the region of hydrogen adsorption potentials (H_{ad}) on Pt-electrodes in aqueous solutions, a surface reaction occurs with the formation of a chemisorbed "reduced form of CO_2 " (rCO_2), which includes, among other species, various forms of CO_{ads} [31–34]. Various authors discuss the composition of rCO_2 on Pt-group metals and their alloys [34], depending on the catalyst nature and the cationic and anionic composition of the electrolyte, the electrochemical mechanism of rCO_2 oxidation, the properties of CO in the rCO_2 composition, and CO_{ads} obtained during the chemisorption of CO that is dissolved in the electrolyte on Pt metals, including a (pc) Pt electrode. Some questions that are related to the oxidation of rCO_2 on Pt also remain open, in particular:

- (1). Whether the features of electrochemical oxidation of rCO_2 into carbon dioxide saturated aqueous H_2CO_3 solution without electrolyte additives can be detected?
- (2). Is there any correlation between the electrocatalytic oxidation and open-circuit oxidation of rCO_2 ?
- (3). Does the oxidation of rCO_2 under electrocatalytic and open-circuit conditions proceed as an oscillatory reaction, and, if so, what useful physicochemical information can be derived from this process?

To date, we have not found any published results on electrocatalytic measurements aimed at identifying the correspondence between the electrochemical and catalytic effects, oscillation effects for the oxidation reaction of rCO_2 .

In accordance with the above, the goal of this work was to identify the relationship and find correlations for the oxidation dynamics of rCO_2 on (pc)Pt in a CO_2 -saturated aqueous solution of "helium washed" water under electrochemical and open-circuit conditions and propose a probable mechanism of the oxidation process under these conditions.

2. Materials and Methods

The measurements under electrochemical and open-circuit conditions were carried out in a glass three-electrode electrochemical cell without separating the cathode and anode space to reduce resistance in the solution at room temperature ($\sim 20^\circ C$). The electrochemical cell was placed in a Faraday box. The supply of the test substance from the side vessel of the cell to its working space was carried out by means of electromagnetic valves or a glass faucet. The solenoid valves were disconnected during the measurements.

A (pc)Pt electrode (99.999%) in the plate form lightly etched in Aqua regia with a geometric surface area $S_g \approx 0.5 \text{ cm}^2$ was used as the working electrode. Before each experiment, the smooth (pc)Pt electrode was cleaned in a mixture of H_2O_2 and H_2SO_4 in a ratio of 1:1; after that it was thoroughly washed with water (Millipore–Merck, $\Omega = 18.2 \text{ MOhm}$) to eliminate the contaminants on the Pt surface. This method of pretreatment of polycrystalline platinum is quite typical for electrochemical studies. The real surface area of the electrode was determined by integrating the anode parts of cyclic voltammograms from 0.06 V (R.H.E.) by the desorption of hydrogen adatoms H_{ad} in solutions of $1.95 \times 10^{-4} \text{ M HClO}_4$ and $0.5 \text{ M H}_2\text{SO}_4$, while assuming that the electricity quantity $q = 210 \mu\text{C}$ was spent per 1 cm^2 of S_r . The obtained values of $Q_{H_{ad}}$ in the selected electrolytes were close to each other. The roughness factor for the pcPt electrode defined as S_r/S_g was ~ 1.7 – 1.8 . The $0.5 \text{ M H}_2\text{SO}_4$ solution was only used to compare the obtained S_r values in the sulfuric acid solution with the values obtained in $1.95 \times 10^{-4} \text{ M HClO}_4$. In order to assess the concentration of dissolved oxygen in water, a Pt-wire soldered into glass was used as the working micro-(pc)Pt electrode (Metrohm) ($d = 10 \mu\text{m}$). Pt wire was used as the counter electrode. A hydrogen electrode in $1.95 \times 10^{-4} \text{ M HClO}_4$ was used as a reference electrode.

The HClO₄ concentration is chosen to bring the pH value of this acid solution as close as possible to pH of the saturated H₂CO₃ solution, which is equal to 3.85.

Water (Millipore–Merck) with $\Omega = 18.2$ MOhm was used as a solvent for all working electrolytes. The water purification was carried out on the Direct-Q3[®]UV (Millipore Corporation, Molsheim, France) device. H₂O and a 1.95×10^{-4} M HClO₄ solution that was prepared by the successive dilution of 70% (wt.) HClO₄ (suprapure, Merck) was used as a background electrolyte. The HClO₄ solution was used as a model “background” electrolyte, because, as, in the case of CO₃²⁻ [35], no specific adsorption of ClO₄⁻ anions occurs on the Pt electrode [36].

At the beginning, the electrochemical cell and then H₂O in the side vessel were thoroughly deaerated by blowing He (Linde-Gas, 99.9999% vol.). According to the available publication [30,37], after a prolonged bubbling of pure He through H₂O, dissolved oxygen and other atmospheric gases remain in water in trace amounts, and the final pH value is equal to ~7. An analysis of cyclic voltammograms (CVA) obtained in water on a micro-Pt electrode showed that the final concentration of residual oxygen in water after blowing He for 1.5 h is minimal and it is not more than $\sim 10^{-9}$ M. The C_{O₂} concentration was determined by the equation for the stationary current $I = nFDc^0\delta$ for the microelectrode [38], where δ is the diameter of the Pt wire, n is the number of electrons (4), F is the Faraday number, I is the measured stationary current at different potential sweep rates with the extrapolation to $v = 0$, D is the diffusion coefficient of oxygen (2.0×10^{-5} cm²/s), and c^0 is the desired C_{O₂} concentration. The preliminary removal of oxygen from H₂O by He made it possible in subsequent catalytic measurements to relate the data on the oxidation of rCO₂ by dissolved O₂ mainly to the residual concentration of oxygen presented in CO₂ after a further purification of carbon dioxide from O₂ impurities on a special filter for gas chromatography.

The resulting deaerated H₂O was saturated with CO₂ in a lateral vessel for 1.5 h. CO₂ at a pressure of 1 bar (99.9999% vol.) being supplied from a CO₂ cylinder (Linde-Gas, 99.9993% vol.) was purified on the SGT-CO1005 filter for gas chromatography. The residual O₂ concentration in an H₂CO₃ solution after purging CO₂ was equal to $\sim 10^{-6}$ – 10^{-7} M. The working electrolyte was a saturated solution of ~ 0.036 M CO₂ (gas) (20 °C) with a pH of 3.85 [39]. Dissolved CO₂, O₂, CO₃²⁻, and H⁺ species are present in significant amounts in aqueous solutions saturated with CO₂ at pH < 4 [40]. Trace impurities of indifferent ClO₄⁻ ions from the reference electrode vessel may also be present.

The working electrolyte that was saturated with carbon dioxide was transferred to the working space of the cell and then measurements were started. The total time of each experiment was >10 h. CO₂ was slowly purged over the solution through a water seal in order to minimize the possible reverse diffusion of atmospheric O₂ through cell connections into the working space and to maintain a steady concentration of the oxidant in the working solution. Electrocatalytic and open-circuit measurements were carried out while using a potentiostat-galvanostat Autolab 100N.

2.1. Electrocatalytic Measurements under Potentiodynamic Conditions

First, the electrode was cycled in the region of potentials E 0.03–1.5 V (10 cycles; $v = 10$ mV/s) with a registration of CVA curves, and the reproducibility of the resulting potentiodynamic curves was achieved, when the currents on the curves differed by no more than 2%. The chosen speed of potential sweep approximated the conditions of the process stationarity. Further, we registered the anodic CVA curve to the complete oxidation potential of chemisorbed rCO₂, changed the potential of the working electrode for the selected potential for the formation and accumulation of rCO₂ in the range of the H_{ad} adsorption potentials, and registered the potentiostatic current transient (I, t —curve) during 400 s. The criterion for choosing the potential delay time (t_d) was determined by the time of achieving the current stationarity on the I, t —curve and the current values in the maxima of the oxidation peaks H_{ad} and rCO₂ when registering the subsequent anode branches of CVA. The selected value of t_d allowed for us to obtain the limit values of the surface coverages

of H_{ad} and rCO on the (pc)Pt electrode at the corresponding accumulation potentials. Further, from the selected accumulation E , the anode branch of CVA was recorded with the corresponding oxidation peaks. Before recording each subsequent potentiostatic I,t -curve of rCO_2 accumulation, intermediate CVA curves (2–3 cycles) were always recorded in the 0.03–1.5 V potential region to control the reproducibility of the electrode surface after rCO_2 oxidation. The amounts of electricity that were spent for the oxidation of H_{ad} and rCO_2 were estimated from the anode currents in CVA. For this purpose, anodic parts of the potentiodynamic curve were integrated in the desorption potentials range of residual H_{ad} in the presence of chemisorbed rCO_2 that was adjusted for the charging current of the double electrical layer (DEL) (the final value – $Q_{H_{ad}}^{rCO_2}$), and in the oxidation potentials range of rCO_2 adjusted for anodic currents of the CVA curve recorded after the potential delay at 0.480 V the final value – Q_{rCO_2} . There is no H_{ad} on the (pc)Pt surface at 0.480 V and, as result, no rCO_2 is formed. In addition, the value is located in the initial region of the oxidation potentials of rCO_2 and, therefore, does not significantly affect the coverage estimates. In the model “background” solution of 1.95×10^{-4} M $HClO_4$, the surface coverage of H_{ad} ($Q_{H_{ad}}$) was estimated by integrating the corresponding anodic CVA in the desorption potentials region of H_{ad} adjusted for the charging current in the region E corresponding to DEL. After that, the dependences of $Q_{H_{ad}}$, $Q_{H_{ad}}^{rCO_2}$, and Q_{rCO_2} on the potentials of accumulation E were plotted, which allowed for us to estimate the coverages of chemisorbed rCO_2 on the surface of the (pc)Pt electrode.

2.2. Catalytic Measurements under Open-Circuit Conditions

The method (see Section 2.1) served as the basis for measuring the transients of the non-current potentials. After achieving the reproducibility of the initial CVA curves during 10 cycles, the potential was switched to 0.880 V (200 s) for the complete removal of chemisorbed substances from the (pc)Pt surface, and then the potential is switched to a chosen value of the corresponding accumulation potentials in the H_{ad} adsorption potentials region during t_d 400 s and the I,t -curve was recorded. Next, the cell was switched off and the E_{nc},t -curve was registered to the E_{nc} value of the potential of the complete rCO_2 oxidation. For the chosen maximum discreteness of points on the recording device, it was necessary to obtain the maximum number of points on the obtained experimental dependences. In addition, it is obvious that the correct mathematical processing of the original E_{nc},t -dependencies required a high reproducibility of experimental data. The reproducibility of the recorded E_{nc}, t -curves was maximal, and deviations in values were <7%.

2.3. Electrocatalytic Measurements under Galvanostatic Conditions

A number of measurements were also carried out under galvanostatic conditions. The basis for the registration method of the galvanostatic chronopotentiometric curves was the method (Section 2.2), with the exception that after the delay of the potential of rCO_2 accumulation, a small anode current was switched on, and the E,t -curve was registered up to the potential of the complete rCO_2 oxidation.

2.4. Other Measurements

We used a scanning electron microscope LEO EVO 50 XVP (Karl Zeiss) with EHT = 25.00 kV and WD = 6.0 and 7.5 mm in order to analyze the morphology of the working electrode surface by the SEM method.

The XRD analysis of Pt was performed using the CCDC database to identify the crystal phases of the (pc)Pt electrode. The data were obtained while using an ARL X'TRA (Thermo Fisher Scientific, Waltham, MA, USA) diffractometer that was equipped with a Theta-Theta goniometer ($CuK\alpha$ -radiation, 40 kV, 40 mA). X-ray diffraction patterns were recorded at the speed of scan 1.2 deg/min in the region of $20 < 2\theta < 70$.

We used a triaxial seismometer Anchar-Geo with the frequency range 0.08–45 Hz, maximum sensitivity not worse than 0.1 nm (at a frequency of 3 Hz), digitization bit rate 24 bits, digitization frequency 92 Hz, and the X-Y-Z coordinate independence up to 50 dB

in order to monitor mechanic vibrations inside the laboratory room with the aim to estimate their influence on the processes occurring in the electrochemical cell.

2.5. Quantum-Chemical Calculations

Preliminary quantum chemical calculations were carried out on the simplest Pt₁₃ cluster in order to only estimate the probability and possibility of process occurring and suggest a likely mechanism and energies for the process of the rCO₂ oxidation reaction. The electronic structure of cluster was calculated by the density functional (DFT) method using B3 as the exchange functional [41], LYP [42], and VWN5 [43] as correlation functionals (U-B3LYP). In order to reduce the calculation time, the SBK pseudo potential [44] and the corresponding basis set supplemented by polarization functions on all atoms were used. All of the calculations were performed while using a Firefly quantum chemical software package [45,46]. The analysis of natural orbital occupation was performed using the NBO software package [47].

3. Results

3.1. Morphology of pcPt Electrode Surface

Figure 1a shows the SEM images of the working (pc)Pt electrode. It can be seen that, after lightly treating the surface of (pc)Pt in Aqua regia and performing the experiment, the surface of the electrode as a whole retained its smoothness in general (Figure 1a). However, a detailed examination of the surface morphology at large magnifications (Figure 1b–f) demonstrates that there are many etching pits on the surface. The grain boundaries did not appear noticeably, but a noticeable number of the etching pits are formed (Figure 1b–f). It can be seen that the resulting etching pits are not randomly distributed, but rather are located along the zones—light and dark areas of the surface. The shape of the etching pits corresponds to a cubic face-centered structure of Pt (Figure 1f). The square base of the etching pits is bounded by octahedra and, in the first approximation, it can be considered to be Pt(111).

Let us consider Figure 1d. We estimated the total number of etching pits with sizes ~26–260 nm. Figure 2 shows the distribution of pits by their size.

We then determined the total surface area shown in Figure 1d, estimated the total surface area related to the etching pits in question, and estimated their contribution to the total surface area of the platinum in question. It turned out that, on the considered surface area, the total area increases by ~10%. Thus, the contribution of defects to the total surface area of polycrystalline platinum is quite significant.

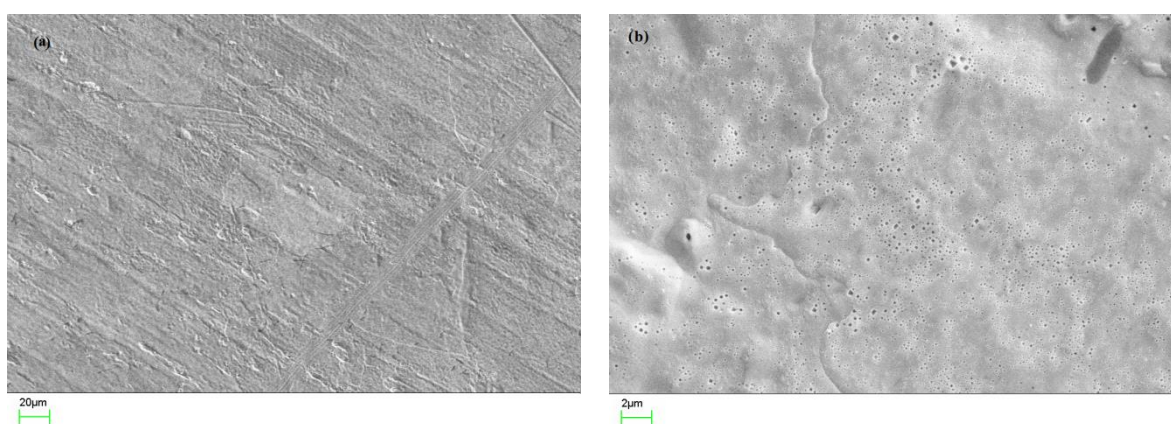


Figure 1. Cont.

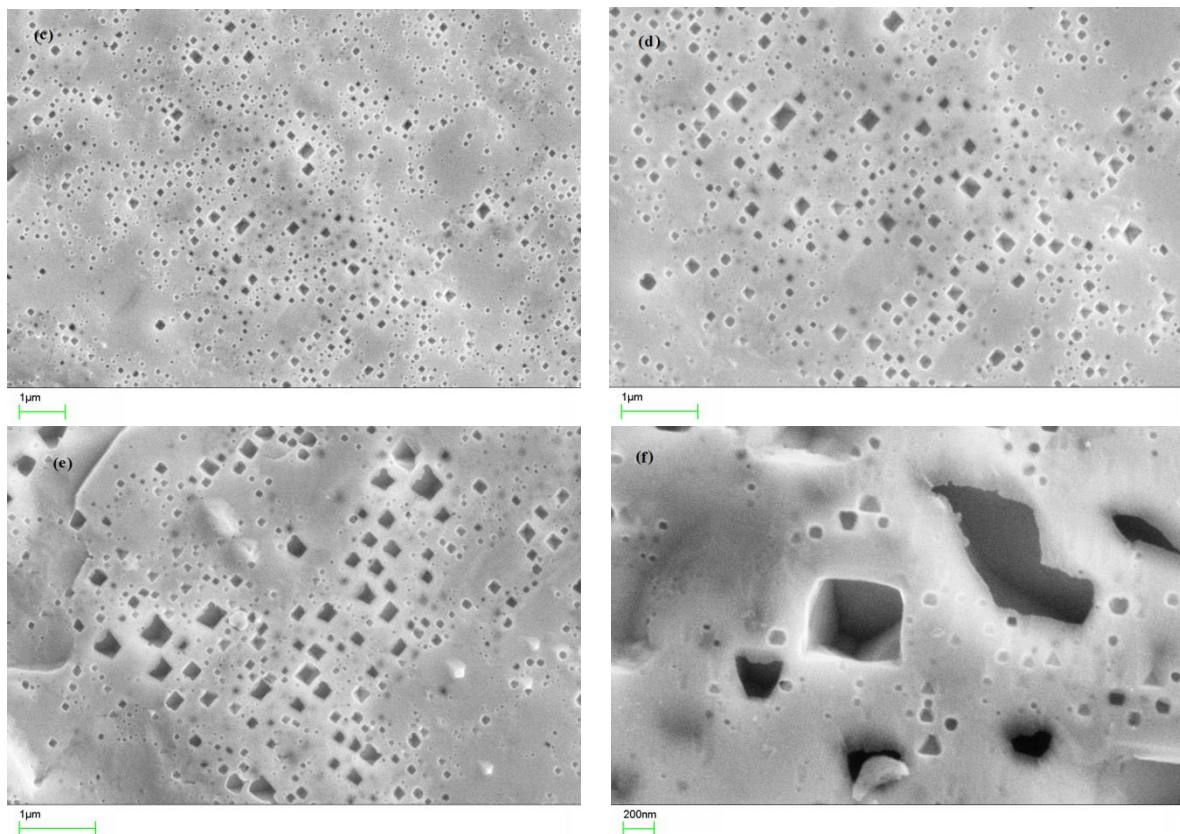


Figure 1. SEM images of the working (pc)Pt electrode of a general view (a) and two sections of the surface (b–d) and (e,f) with WD = 7.5 mm (a–d) and WD = 6.0 mm (e,f) at different magnifications: 1000× (a); 10,000× (b); 30,000× (c); 50,000× (d,e) and 100,000× (f).

It is obvious that the distribution of defects may be different at other areas of the (pc) Pt surface, and the number of defects may differ both up and down. The appearance of etching pits can be caused by both the influence of etching of the electrode in Aqua regia and influence of chemisorbed $r\text{CO}_2$. Based on the obtained SEM data, it is impossible to clearly identify the effect of adsorbed $r\text{CO}_2$ on the surface morphology of Pt. This task will require further research and it was not a part of the presented work.

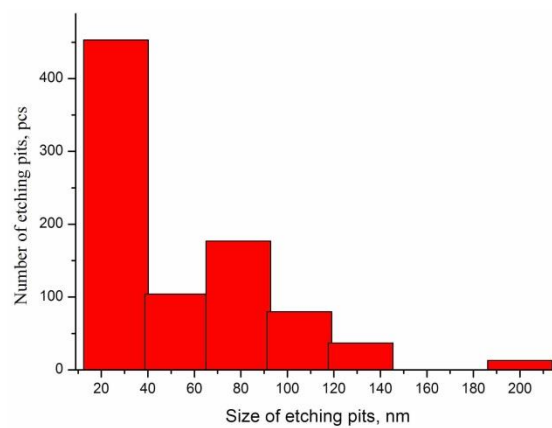


Figure 2. The distribution of the pits by their size for Figure 1d.

3.2. Electrochemical Oxidation of $r\text{CO}_2$ under Potentiodynamic Conditions

Figure 3a shows the anode branches of CVA curves in water saturated with CO_2 in the potential region of 0.03–1.5 V.

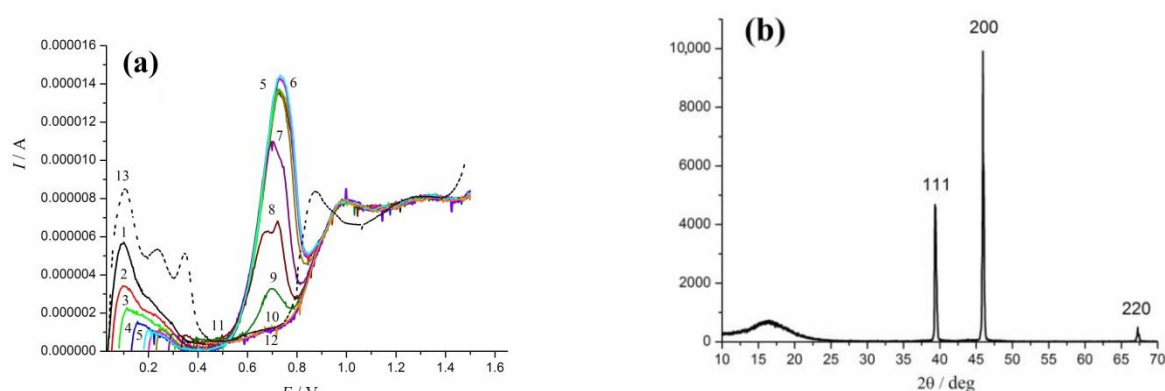


Figure 3. Anode branches of cyclic voltammograms (CVA) curves (a) in water saturated with CO_2 after the delay of potentials E in Volts (the number of curve): black line: 0.03 (1); red line: 0.05 (2); green line: 0.08 (3); blue line: 0.130 (4); cyan line: 0.180 (5); magenta line: 0.200 (6); dark yellow line: 0.230 (7); purple line: 0.280 (8); wine line: 0.330 (9); olive line: 0.380 (10); orange line: 0.430 (11); violet line: 0.480 (12). Dotted black line (13): anode branch of CVA curve in 1.95×10^{-4} M HClO_4 solution after a delay of the initial potential of 0.03 V. Scan rate 0.01 Vs^{-1} . (b) The diffractogram for (pc)Pt electrode.

The cathodic branches of the obtained CVA curves coincide and they are not presented here. After the $E = 0.03$ V delay, the oxidation of a small amount of molecular H_2 formed at this potential at the initial stage of the hydrogen evolution reaction is observed, in addition to the H_{ad} oxidation. In the H_{ad} desorption potentials region 0.05–0.35 V (Figure 3a) after the corresponding E delays, one can see the desorption peaks of H_{ad} appearing on the anode curves and corresponding to the oxidation of residual H_{ad} remaining on the (pc)Pt-surface after the formation of chemisorbed rCO_2 . The Pt(111) face is maximally inert with respect to CO_2 adsorption and, consequently, the formation of rCO_2 on this face is difficult, according to T. Iwasita [48]. It can be seen, from the diffractogram obtained by the XRD method for the (pc)Pt electrode (Figure 3b), that the Pt(111) facet contribution is significant. Therefore, there is a sufficient number of sites on the surface of the (pc)Pt electrode that are not available for the formation of rCO_2 , but are available for the adsorption of H_{ad} , which is consistent with the data of Figure 3a. The complete oxidation potential of rCO_2 , according to Figure 3a, is equal to ~ 0.88 V. A significant width of the oxidation peaks of rCO_2 (up to ~ 0.4 V) may indicate the energy heterogeneity of the Pt surface.

The CVA curves for rCO_2 oxidation are close to CVA that was obtained earlier in the works of B.I. Podlovchenko, T. Iwasita [35,49], and other researchers [34] in background solutions of various acids without the strong anion adsorption, but at lower pH values. Therefore, the pH values in our measurements did not fundamentally affect the shape and position of the oxidation peaks of rCO_2 on CVA, and the energy of the process in a wide range of acidic pH values is close. Obviously, in a saturated solution of H_2CO_3 , it is impossible to obtain a background curve to estimate the surface coverage of H_{ad} , because dissolved gaseous CO_2 is always present. Therefore, a model “background” system 1.95×10^{-4} M HClO_4 was chosen in order to assess the surface coverages (see the method section). Figure 3a shows the anode branch of the CVA curve, which is recorded in the 1.95×10^{-4} M HClO_4 solution after a delay of the initial potential of 0.03 V (as shown with the dotted line).

Double oxidation peaks are observed on some CVA curves (Figure 3a). The delay on the CVA curves that were recorded from the potential values of 0.23 and 0.28 V corresponding to the region of medium coverages is manifested as the presence of the double rCO_2 oxidation peaks in the transition region in the vicinity of 0.6 V. The peak doubling is weakly manifested on the potentiodynamic curves that were obtained after the E delays in the region of high coverages (< 0.23 V) (Figure 3a). However, after differentiating these curves (Figure 4), it is possible to see that there are also small delays near 0.6 V. The electrochemical oxidation of H_{ad} and rCO_2 obeys the exponential dependence of I versus E , the parts of which are linearized in the region of the desorption potentials of H_{ad} and oxidation of rCO_2 in the $\lg I, E$ coordinates.

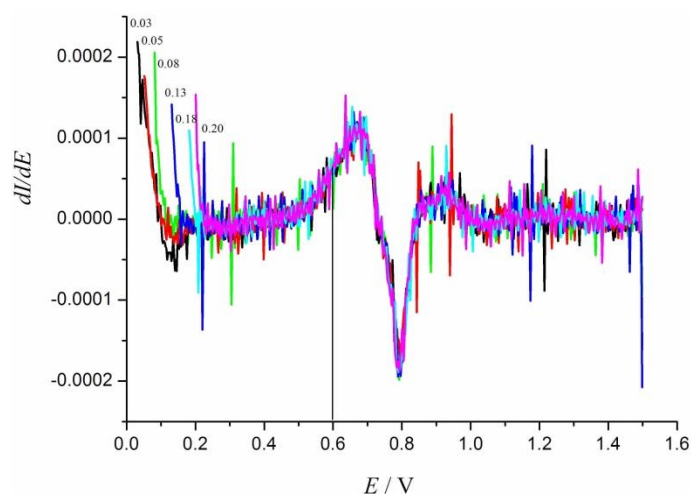


Figure 4. Anode branches of CVA curves in dI/dE scale after the delay of potentials (E in Volts). Black line: 0.03; red line: 0.05; green line: 0.08; blue line: 0.13; cyan line: 0.18; magenta line: 0.20. Scan rate 0.01 Vs^{-1} .

Figure 5 presents the Tafel dependence of the slopes for the $r\text{CO}_2$ oxidation ($R = 0.995$) for the CVA curve that was obtained after a delay of 0.08 V. It is evident that the slope equals 0.099 V in the region of potentials 0.5–0.6 V, thereafter the slope increases and reaches 0.165 V in the 0.6–0.7 V range.

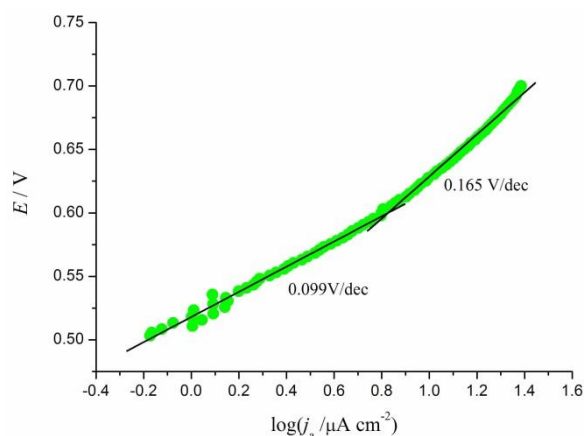


Figure 5. Tafel plots (black line) for the anodic CVA part of $r\text{CO}_2$ oxidation in water saturated with CO_2 after the delay of $E = 0.08 \text{ V}$ (green circles).

The Tafel dependences were obtained at nonstationary conditions. However, the $r\text{CO}_2$ oxidation dynamics is obviously markedly different after passing the critical value of 0.6 V. A number of papers have discussed the reasons for the existence of the maxima during CO oxidation [28], but the unambiguous cause of this effect has not been determined. Two oxidation regions are usually considered: the regions of 0.35–0.6 V (R.H.E.) before the oxidation peak [50–53] and from 0.6 V to higher potentials [54–58]. The authors [57] suggested, on the basis of differential electrochemical mass spectrometry data, that the changes of the Tafel slope at the variation of the scan speed are caused by the changes in the degree of the Pt surface coverage by OH particles and not by different CO oxidation mechanisms. A more detailed discussion of the oxidation mechanism is presented in the Discussion section. Thus, the obtained differences in the slopes of the Tafel dependences at 0.6 V qualitatively coincide with the literature data.

On the basis of the data that were obtained from oxidation peaks, the dependences $Q_{r\text{CO}_2}$, E were plotted (Figure 6a). The dependences for the residual H_{ad} desorption

(Figure 6b) are linearized in the coordinates $\ln Q, E$, which corresponds in the first approximation to the Temkin isotherm of the H_{ad} adsorption on Pt.

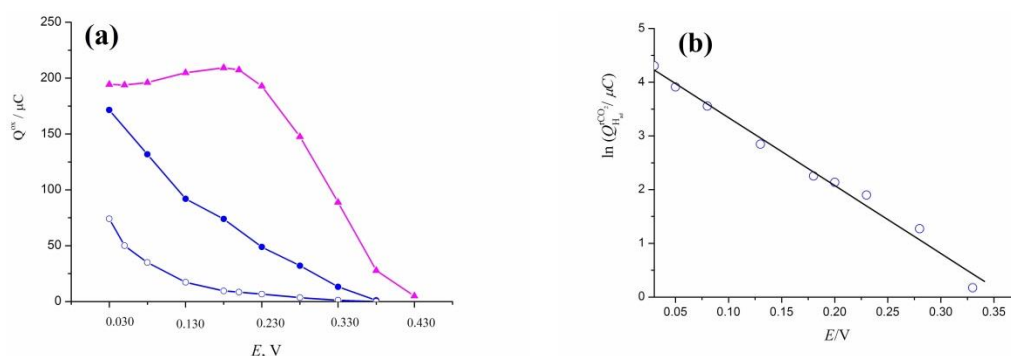


Figure 6. Charges (a) Q^{ox} of the oxidation: magenta triangles: Q_{rCO_2} ; blue circles: $Q_{H_{ad}}$; blue rings: $Q_{H_{ad}}^{rCO_2}$. Charges (b) of the H_{ad} oxidation in the presence of rCO_2 in $\ln Q_{H_{ad}}^{rCO_2}, E$ scale.

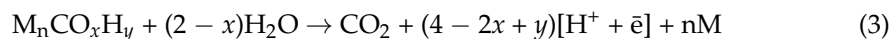
It can be seen from Figure 6a that there is a transition region of values Q_{rCO_2} in the region of potentials 0.180–0.200 V. In the potentials range <0.180 V, Q_{rCO_2} reaches the limit value. The estimate of the adsorbed amount of rCO_2 in the range of high coverages gives the value of $\sim 3 \mu g$ ($\sim 0.1 \mu M$), assuming that the main product of the CO_2 recovery is CO. Taking the amount of electricity consumed to oxidize the residual H_{ad} into account, the total surface coverage of rCO_2 is equal to $\sim 0.7 \pm 0.05$ of the monolayer. This value is consistent with the literature data for Pt [34]. If we assume that the main components in rCO_2 are chemisorbed molecules of CO_{ads} , which exist in the bridged (b) and/or in the linear (l) forms bound to (pc)Pt, and also make the correction for the S_r surface that is occupied by residual adsorbed hydrogen (the final value of S_r equals $\sim 0.54 \text{ cm}^2$ in this case), then we can write the ratio to determine the contributions of the currents that correspond to these two different forms of chemisorbed CO in the total oxidation current of rCO_2 for the case of the mixed forms of CO_{ad} interacting with Pt atoms on the surface of the pcPt electrode that are not occupied by H_{ad} :

$$420 \cdot \theta_{CO(l)} + 210 \cdot \theta_{CO(b)} = Q_{ox} [\mu C / \text{cm}^2], \quad (1)$$

$$\theta_{CO(l)} + \theta_{CO(b)} = 1, \quad (2)$$

where $\theta_{CO(l)}$ is the monolayer fraction of CO_{ads} in the linear form, $\theta_{CO(b)}$ is the monolayer fraction of CO_{ads} in the bridged form, and Q_{ox} is the amount of electricity that is required for the oxidation of the CO_{ads} monolayer. The assessment of the contributions of each form of chemisorbed carbon monoxide molecules into Q_{ox} showed that, in the case of high coverages at the potentials 0.03–0.230 V, the fraction of $CO_{(l)}$ is between ~ 0.71 (0.230 V) and 0.84 (0.180 V) of the monolayer capacity, i.e., the CO_{ads} mainly exists in the linear form. In the case of the medium coverages (0.280 V), the fraction of $CO_{(l)}$ decreases markedly and reaches the value of 0.3 of the overall capacity of the monolayer. In the region of low coverages, the fraction of $CO_{(l)}$ generally takes negative values, which is meaningless from a physical point of view, if we consider the CO_{ads} adsorption on the surface of the (pc)Pt electrode as a monolayer. This may mean that, in addition to CO_{ads} , there may be other particles in the l- and/or b-forms, for instance, triple-bonded bridged CO, that are not taken into account in (1). Indeed, three forms of CO_{ads} were recorded by the in-situ FTIRS method on a (pc)Pt electrode in a 0.5 M H_2SO_4 solution saturated with CO_2 , with the absorption band at 1991 cm^{-1} corresponding to $CO_{ads(l)}$, which at 1854 cm^{-1} assigned to multi-linked CO_{ads} and the band at 1878 cm^{-1} attributed to $CO_{ads(b)}$ [49]. The obtained data correspond to the data for particles that were adsorbed from the gas phase. In an 0.5 M $HClO_4$ solution, COOH and COH particles were also observed [49]. The $CO_{ads(l)}$, $CO_{ads(b)}$ and CO in the multi-linked form, as well as COH and HCOO species were detected in other studies [48,59] on Pt. The possible chemical composition of rCO_2 on the Pt surface is

discussed and described in detail [34], namely: CO, COOH, CHO, COH, C(OH)₂, (H, CO₂, H₂O) according to the data of various methods of surface characterization. Currently, the net rCO₂ oxidation reaction is described, as follows [34]:



Some preliminary information regarding the nature of the adsorbate can be obtained from the analysis of the value of eps (electron per site) as the number of electrons involved in the oxidation of the adsorbate accommodated at one site at the surface:

$$\text{eps} = (4 - 2x + y)/n \quad (4)$$

According to the equation that was proposed by Tokarz [60]:

$$\text{eps} = \frac{Q_{rCO_2}}{\Delta Q_{H_{ad}}} \cdot \theta_{H_{ad}}, \quad (5)$$

where Q_{rCO_2} is the amount of electricity that is required to oxidize rCO₂, $\Delta Q_{H_{ad}}$ is the difference between the amount of electricity consumed in the oxidation of H_{ad} in the absence and in the presence of rCO₂, and $\theta_{H_{ad}}$ is the surface fraction covered by H_{ad}. The calculations by Equation (5) on the basis of Figure 6 allowed for us to estimate the eps values that are given in Table 1.

Table 1. Determination of eps in the CO₂–H₂O system on the (pc)Pt electrode according to the data presented in Figure 4.

<i>E</i> , V	$Q_{H_{ad}}$, μC	$Q_{H_{ad}}^{rCO_2}$, μC	Q_{rCO_2} , μC	$\Delta Q_{H_{ad}}$, μC	$\theta_{H_{ad}}$	Eps
0.03	171.45	74.06	194.38	97.39	1.00	1.99
0.08	131.75	34.96	196.09	96.79	0.77	1.56
0.13	91.97	17.25	204.88	74.72	0.54	1.48
0.18	73.94	9.51	209.26	64.43	0.43	1.40
0.23	48.84	6.69	192.86	42.15	0.29	1.33
0.28	32.08	3.57	147.50	28.51	0.19	0.98
0.33	13.21	1.19	88.85	12.02	0.08	0.59
0.38	1.10	0.03	27.78	1.07	0.01	0.26

According to the data that are presented in Table 1, the eps values are within 1.99–1.4 for the range of high coverages (0.03–0.18 V). In the range of medium age (0.23–0.28 V), the eps values are varying within 1.33–0.98 and they decrease to 0.59–0.26 in the range of low coverages (0.33–0.38 V). In this case, according to the data (Figure 5 in the publication [34]), the formation of PtCO particles can be expected on the surface of (pc)Pt in the range of high coverages, whereas Pt₂CO, PtCOOH can be formed at medium coverages and Pt₃COH and Pt₃CO species in the region of low coverages. These species were observed [49] by FTIRS in other electrolytes. In this case, the electrochemical reduction of CO₂ on Pt can be expected in accordance with the following net reactions [34] for CO_(l) ($n = 1$), CO_(b) ($n = 2$) and CO in the multi-bonded form:



for COOH:



and for COH:



The final answer to the question of what is the nature of the particles together with CO_{ads} could be included in the rCO₂ forms in our experimental conditions should be given

by using other, non-electrochemical, spectroscopic methods that are applied for the study of the Pt surface in a saturated solution of carbonic acid. The obtained eps values (Table 1) are consistent with the eps values that were earlier obtained for Pt [61].

At the values of potentials E in the vicinity of 0.200 V, there is a transition from medium to high coverages of $r\text{CO}_2$, where some increase in the amount of electricity $Q_{r\text{CO}_2}$ spent for oxidation of $r\text{CO}_2$ is observed (Figure 6a). The “anomalous” increase in the initial rate of CO_{ads} formation from CO_2 on Pt(110), Pt(331) and Pt(221) surfaces of Pt electrodes was found at the adsorption potential of 0.2 V (R.H.E) in an 0.1 M HClO_4 solution [1]. The phenomenon of a sharp transition from medium to high coverages during the adsorption of CO from the gas phase at 310 K for the work function change of 200 mV was observed at Pt(100) [62]. These effects can probably be explained not only in terms of the influence of the Pt surface structure [1], but also by the influence of the electronic structure of Pt with respect to chemisorbed CO [63]. By using in situ SFG spectroscopy, the authors identified this critical region of CO chemisorption potentials and showed that there is a maximum resonance effect between the Fermi electron level of a Pt electrode with an anti-bonding $5\sigma_a$ orbital of chemisorbed CO in the vicinity of $E = 0.2$ V. Thus, the binding energy between CO_{ad} molecules and Pt surface is maximal in this region of E values.

Thus, the electrochemical data that were obtained by us in a moderately acidic solution of saturated H_2CO_3 are in good agreement with the previously obtained data for the region of low pH values in the absence of specific adsorption. This allowed for us to refer the investigated system to the classical electrochemical system and proceed further to the catalytic measurements on the oxidation of adsorbates on the (pc)Pt electrode under galvanostatic and open-circuit conditions of measurements in the studied solution.

3.3. Oxidation of $r\text{CO}_2$ under Galvanostatic and Open-Circuit Conditions

Figure 7a depicts a number of galvanostatic potentiometric oxidation curves (curves 2–5) recorded after the accumulation of $r\text{CO}_2$ at $E = 0.08$ V under conditions of small currents (0.101–1.189 μA).

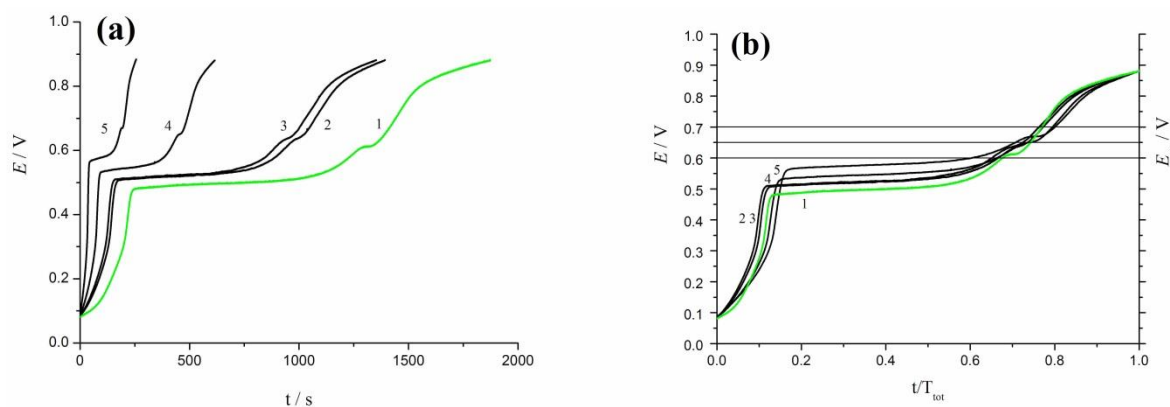


Figure 7. (a) Transient of non-current potential (green lines) (1) and galvanostatic potentiometric curves (black lines) at set DC (μA): (2)—0.101; (3)—0.161; (4)—0.437; and, (5)—1.189, in water saturated with CO_2 solution after $r\text{CO}_2$ accumulation at $E = 0.08$ V. (b) Corrected transients of non-current potential (green line) (1) and galvanostatic potentiometric curves (black lines) at set DC (μA): (2)—0.101; (3)—0.161; (4)—0.437; and, (5)—1.189, in water saturated with CO_2 solution after $r\text{CO}_2$ accumulation at $E = 0.08$ V in $E,t/T_{\text{tot}}$ scale.

The chosen potential value corresponded to the value E providing high surface coverages, whereas hydrogen was present in the adsorbed form H_{ad} . The shape of the curves qualitatively coincides with the corresponding curves that were obtained earlier by Breiter [32]. The proximity of curves 2 and 3 is obviously due to small differences in the values of the external current. As the value of the set current increases, the time to reach the oxidation potential of $r\text{CO}_2$ decreases, and the delay potential in the vicinity of 0.6 V shifts to the region of more positive potential values.

Figure 8a presents E_{nc} - t -curves in the H_2CO_3 saturated solution. The selected values of the accumulation potentials corresponded to the region of high, medium, and low coverages of rCO_2 . The general view of the obtained transients is qualitatively similar to the galvanostatic chronopotentiometric curves presented in Figure 7a. However, the total time that is necessary to reach the oxidation potential of rCO_2 on Pt in the reported electrochemical galvanostatic conditions was substantially less than in our open circuit conditions.

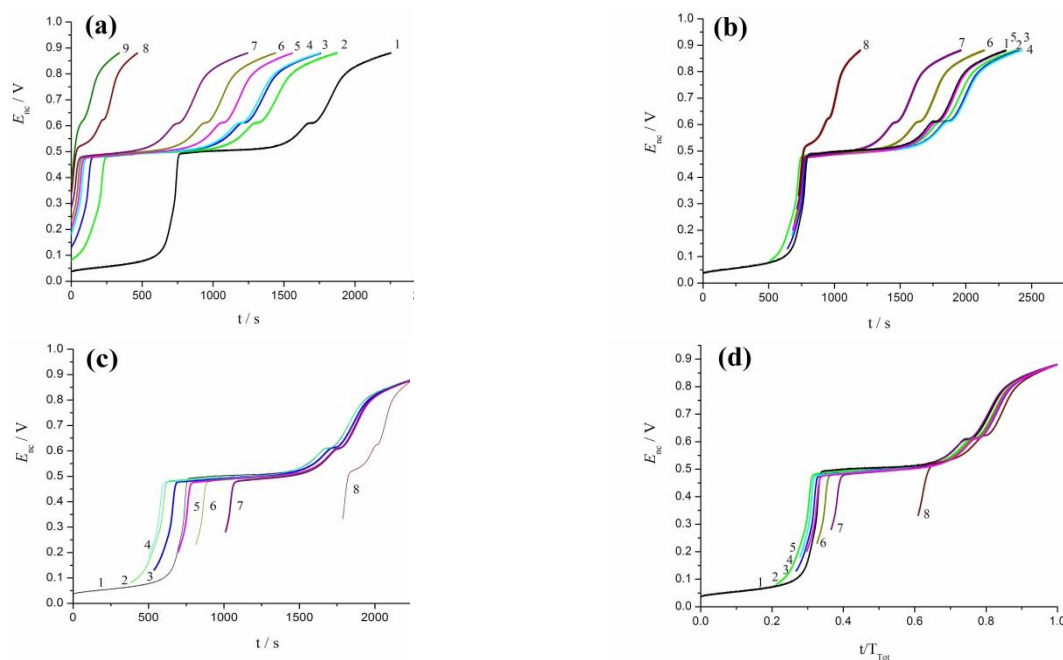


Figure 8. (a) Transients of non-current potential in water saturated with CO_2 after the delay of potentials E in Volts (the number of curve): black line: 0.03 (1); green line: 0.08 (2); blue line: 0.130 (3); cyan line: 0.180 (4); magenta line: 0.200 (5); dark yellow line: 0.230 (6); purple line: 0.280 (7); wine line: 0.330 (8); and, olive line: 0.380 (9). (b) Corrected transients of non-current potential by the shift each of the curves (Figure 8a) on the t -axis at the corresponding times of achievement of their initial individual values of the starting potentials on the curve registered from 0.03 V. (c) Corrected transients of non-current potential by the shift each of the curves (Figure 8a) on the t -axis by the value Δt to reach the complete oxidation potential of rCO_2 . (d) Normalized corrected curve (Figure 8c) for the individual total T_{tot} time to reach the E_{nc} potential of complete oxidation of rCO_2 .

When correcting the obtained curves (Figure 7a) for the total time that is required for reaching the oxidation potential (~ 0.88 V) (Figure 8b), one can see that the curve 1 (Figure 7a) recorded under open-circuit conditions from 0.08 V is close to the curves obtained under galvanostatic conditions at the lowest current values (0.1 and 0.16 μA , curves 2, 3 in Figure 7a).

In this case, the slopes of the curves that were obtained under different measurement conditions are close to each other. At larger values of the set anode currents, the difference between curves 4, 5 and curve 1 (Figure 7b) is more pronounced. Figure 8a demonstrates that the initial part of the curves in the potential region < 0.35 V corresponds to the oxidation of residual H_{ad} species, and the curve then reaches a plateau that corresponds to the potential region of DEL. A similar course of the dependence is observed for curves 2, 3 (Figure 7a). At $E \sim 0.48$ – 0.5 V, the oxidation of rCO_2 begins to manifest, a small potential delay is observed in the vicinity of $E \approx 0.6$ V, after which the oxidation of rCO_2 continues. The potential delay on galvanostatic potentiometric curves (curves 2, 3 Figure 7a) is slightly shifted by ~ 0.025 V to the region of higher anode potential values. Adsorption of OH_{ad} on Pt occurs at potentials above 0.6 V [64,65]. The comparison with the data of [64,65] is correct, because the potential scale used in our work (the pH value of the solution in the vessel of the comparison electrode is close to the pH value of the working electrolyte, with

no specific adsorption of anions) does not differ very much from the potential scale of the reversible hydrogen electrode used in [64,65]. The final part of the transient at $E > 0.85$ corresponds to the oxygen adsorption region (according to Figure 3a) [64,65]. The curves that were recorded from 0.03 and 0.05 V in Figure 8a are characterized by a long initial period due to the oxidation of residual H_{ad} and a small amount of molecular H_2 that formed in electrochemical conditions during the accumulation of rCO_2 at E located in the region of the potentials of the initial part of the hydrogen evolution reaction (according to Figure 3a). We will see that the corrected initial experimental curves are divided into groups if we shift each of the resulting curves in Figure 8a to the right on the t -axis at the corresponding times of achievement of their initial individual values of the starting potentials on the curve registered from 0.03 V (Figure 8b). The obtained transients are almost identical for accumulated forms of rCO_2 in the potentials region of high coverages. For oxidation curves of the rCO_2 forms that accumulated at potentials in the region of medium and low coverages, the time necessary to reach the full oxidation potential of rCO_2 is markedly reduced. The time that is required for reaching the complete oxidation potential of the chemisorbed substance (at a constant concentration of an oxidant in the solution) is determined by the adsorbate amount on the Pt surface. Therefore, obviously, in the case of high coverages, when the amounts of oxidizable substances are close (Figure 6a), the E_{nc} , t -curves should coincide. Additionally, then, in the region of low and medium coverages of rCO_2 (Figure 6a), the achievement time of the complete oxidation potential (Figure 8b) should be decreased. If we shift the original curves (Figure 8a) on the t axis to the right by the value Δt to reach the complete oxidation potential of rCO_2 (Figure 8c), then we will see that the slopes of the sections of the curves in the oxidation region of rCO_2 coincide. However, if we will normalize each corrected curve (Figure 8c) for the individual total T_{tot} time to reach the E_{nc} potential of complete oxidation of rCO_2 , then all of the thus obtained corrected E_{nc}, t -dependences practically coincide in the region of oxidation potentials of rCO_2 (Figure 8d). This means that the mechanism of catalytic oxidation of rCO_2 is the same, regardless of the selected initial values of the accumulation potentials. The previous stage of oxidation of the residual H_{ad} does not affect the mechanism of the subsequent stage of oxidation of rCO_2 in the general oxidation process, and these processes are separated in the time scale.

Figure 9a–c show anamorphoses (anamorphosis is a coordinate transformation that provides piecewise linear approximations of empirical data and allows one to determine the system of critical points where the process mechanism is changed; this approach is widely used in the nomography [27]) for the transient of the non-current potential, which was recorded from the starting value 0.08 V in the $\ln E_{nc}$, t (Figure 9a) and E_{nc} , $\log(t/T_{tot})$ (the part of transient) (Figure 9b) scale, respectively, and Figure 9c shows the part of this transient in the $dE/dt, t$ scale. It can be seen that the obtained curve is described by linear sections of slopes, which differ sharply for the H_{ad} and rCO_2 (Figure 9a) oxidation stages. In the case of the oxidation stage of rCO_2 , the logarithmic slopes also differ in the potentials regions <0.6 V and >0.6 V (Figure 9a) and they are equal to 0.00085 and 0.00141, respectively. Additionally, in the case of the oxidation stage of rCO_2 , the slopes of curves clearly differ in the potentials regions <0.6 V and >0.6 V (Figure 9b,c).

This means that the process rate decreases in the region >0.6 V, as in the case of electrochemical measurement under potentiodynamic, galvanostatic as open-circuit conditions (Figures 5, 7 and 8). It can be assumed that the change in the slope of the straight lines is due to the participation of some new limiting processes in the rCO_2 oxidation reaction at $E > 0.6$ V, in particular, the participation of adsorbed oxygen forms in the rCO_2 oxidation, as it has been already mentioned above. This will be discussed in more detail in the Discussion section.

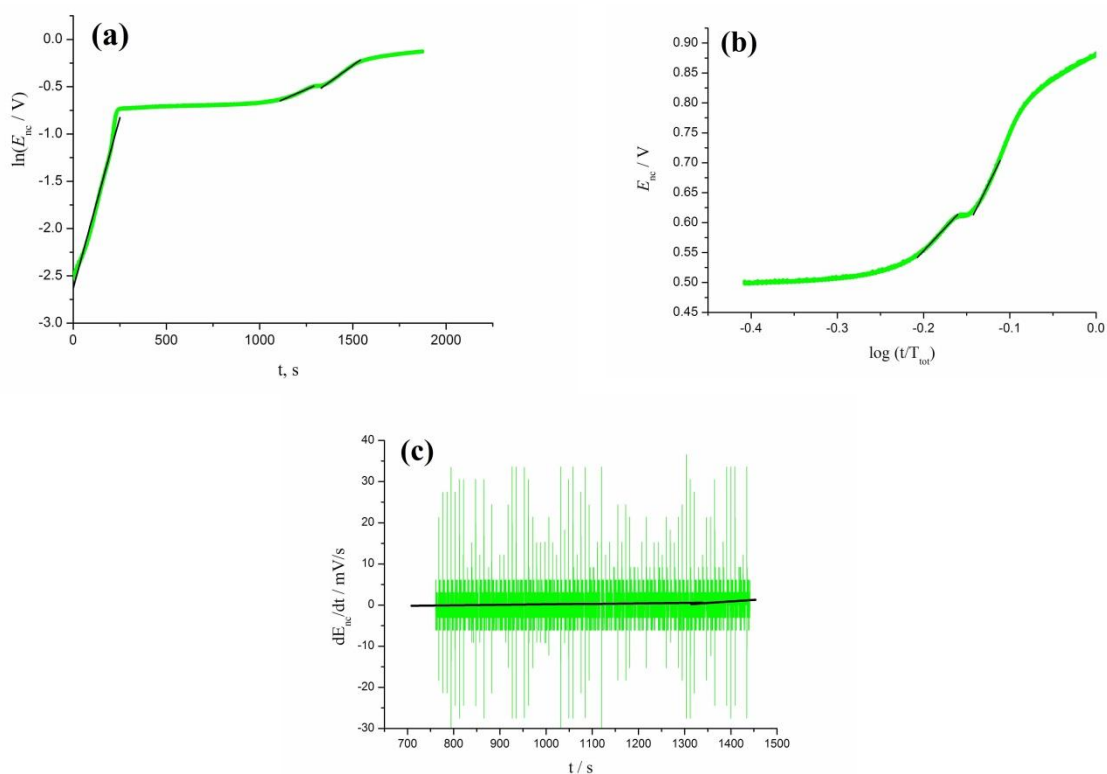


Figure 9. (a) Anamorphoses for the transient of the non-current potential, which was recorded from the starting value 0.08 V on Figure 6a in the $\ln E_{nc}, t$ scale (a) and parts of this transient in $E_{nc}, \log(t/T_{tot})$ (b) and the $dE/dt, t$ (c) scales.

3.4. Oscillation Effects in Oxidation of rCO_2

The analysis of the I, E, E, t , and E_{nc}, t curves revealed oscillations for all of the experimental curves presented in Figures 3a, 7a and 8a correspondingly. As an example, the only transient of the potential is presented in Figure 10a–c, which is registered from the starting potential 0.08 V under open-circuit conditions with some separate parts shown in Figure 10a–c. This paper does not consider a detailed analysis of the observed effects.

The application of mathematical analysis in [27] for the ROH oxidation to the revealed fine oscillations allowed one, for the first time (a), to detect differential characteristics of the processes, such as the locations of critical points at the boundaries of consecutive stages, linear trends for each separate stage, and corresponding slopes and (b) to find the maximum level of reliability upon the data transformations into a linear form and characteristic almost-periods for each of the identified reaction stages. On the basis of the latter, it became possible to determine three consecutive stages of the catalytic oxidation process for CH_3OH and two consecutive stages for C_2H_5OH , $n-C_3H_7OH$, $n-C_4H_9OH$, and $n-C_5H_{11}OH$ with individual oscillations for each of the stages under open-circuit conditions. Furthermore, such a mathematical approach made it possible to separate slow and fast processes, and to propose a general dynamic model of oxidation of alcohol homologs by adsorbed oxygen (it was problematic [20] to obtain more detailed information regarding the chemistry of the alcohol oxidation process, for example, by differentiating the experimental smooth E_{nc}, t -dependences, since the oscillations for different sites were inhomogeneous, and there were no correct criteria for differentiation).

It is seen (Figure 10a–c) that the values of the oscillation periods are close to each other for the whole curve in the entire potential range, and the oscillations are uniform. The total number of complete near-periods (the near-period τ is the value closest to the period at which the value of the shift function—Johnson function [66] $a(\tau)$ —takes minimum values [27]) is equal to 11 for all selected parts with a time interval of 100 s. The durations of the near-periods are equal to ~ 8.5 s (0.118 Hz) and ~ 0.4 s (2.5 Hz) in the entire region of potentials for investigated compounds, and they are obtained by the trend elimination

while using the shift function in accordance with literature data [27]. The obtained values of near-periods are the same for all the transients presented in Figure 8a and they do not depend on the starting value of the potential.

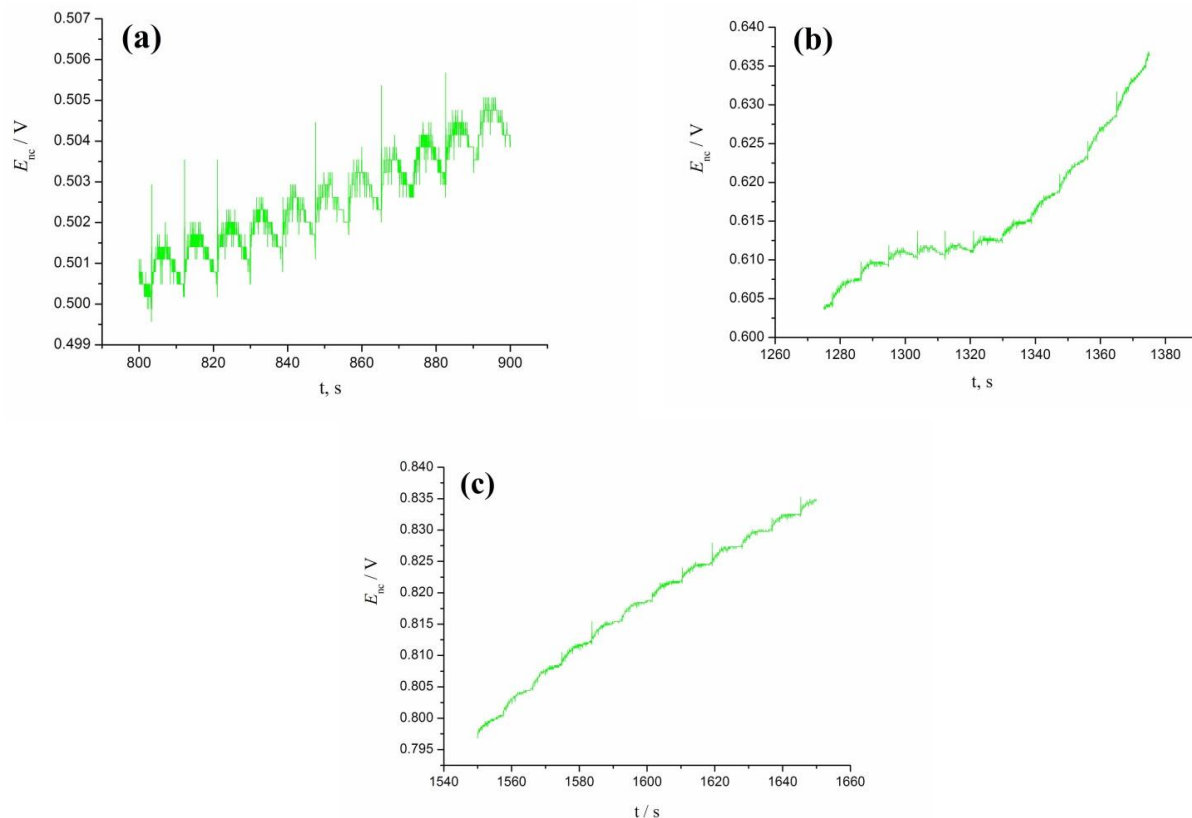


Figure 10. (a–c) Different parts of the transient of the non-current potential, which was recorded from the starting value 0.08 V on Figure 8a.

We carried out similar measurements using the standard equivalent of the electrochemical cell (Dummy cell) for the potentiostat–galvanostat Autolab in order to exclude the possible influence of the measuring device on the oscillations in the experimental system. It turned out that the oscillations that were recorded for the Dummy cell differed dramatically from the oscillations that were obtained upon rCO₂ oxidation. In contrast to catalytic measurements, only high-frequency oscillations were recorded with the Dummy cell, which significantly differed in the shape from the oscillations in the studied system on (pc)Pt. To exclude the possible influence of mechanical vibrations inside the laboratory room, we carried out measurements while using a triaxial seismometer Anchar-Geo. It turned out that the microseismic background in the laboratory and on the laboratory table corresponded to normal laboratory conditions. The overwhelming component in this background was the stable presence of constant vibrations of a small level, in the range of approximately tenths of a micron at a frequency of about 16–17 Hz. These vibrations are caused by the asynchronous electric motors of the ventilation system of the entire building and usually do not cause problems. As to the electrochemical cell under study, these vibrations do not influence in any way and there are no electrical vibrations with this frequency. At frequencies that are below 11 Hz, no specific fluctuations are observed in the microseismic background and its spectrum has the appearance of white noise of a sufficiently low level. Therefore, there was no reason to believe that these weak mechanical vibrations, which have a random noise character, can be the cause of the observed electrical oscillations in the electrochemical cell, which have a strictly regular character in this frequency range. This allowed for us to conclude that the recorded oscillations for the curves presented in Figure 10 mainly responded to electrocatalytic and catalytic processes

occurring on the surface of (pc)Pt and they were not related to the device interference and mechanical vibrations.

The homogeneity of the obtained oscillations (Figure 10a–c) is markedly different from the inhomogeneity of oscillations for the case of oxidation of ROH by adsorbed oxygen on Pt under open-circuit conditions [27]. This means that the stages of the process in the oxidation of adsorbed particles as different in nature as H_{ad} and rCO_2 are not manifested in the case of homogeneous oscillations. Therefore, it can be assumed that the observed homogeneous oscillations (Figure 10) have a self-oscillatory nature and can be caused, for example, by concentration fluctuations of the oxidizer located in the volume of the solution in the near-electrode layer and do not depend on the concentration and nature of adsorbates with reducing properties, i.e., H_{ad} or rCO_2 .

4. Discussion

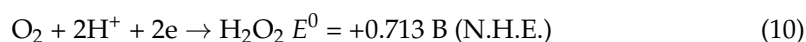
The analysis of transients of the non-current potential, galvanostatic potentiometric curves, and anodic branches of the CVA curves for the oxidation of rCO_2 revealed the fundamental common feature of energy characteristics of the rCO_2 oxidation on the (pc)Pt electrode under open-circuit (catalytic measurements) and electrochemical conditions, i.e., at a small speed sweep of potentials in potentiodynamic measurements and small values of the specified currents in galvanostatic measurements.

Currently, two main interpretations are used when discussing the mechanisms of the electrochemical oxidation of rCO_2 : either H_2O [34,61] or OH^\bullet [67–69] is considered as an oxidant. According to the publication [28], when considering the mechanism of oxidation of CO_{ads} with the participation of OH_{ads} , it was noted that the nature of these particles is not clear.

Two conjugate processes are observed during the oxidation of H_{ad} and rCO_2 on the surface of the Pt electrode under the conditions of electrochemical and catalytic measurements in an aqueous solution: on the one hand, this is the oxidation of these adsorbed substances and, on the other hand, the reduction of dissolved oxygen. Correlating the kinetics of the rCO_2 oxidation process with the kinetics of the conjugate ORR under open-chain conditions is not an easy task, since, *a priori*, we do not know what are the kinetics of the conjugate reduction of dissolved O_2 under open-circuit conditions. The kinetics of ORR on Pt has not yet been fully studied and is debatable; in particular, it is not known under what conditions the complete reduction of molecular O_2 to H_2O occurs with the participation of four electrons, and under what conditions the process ends at the stage of formation of H_2O_2 with the participation of two electrons. On the part of the Pt surface that is free from rCO_2 , processes of electrochemical reduction of soluble O_2 may be described by the following net reaction at low pH values [70–73]:



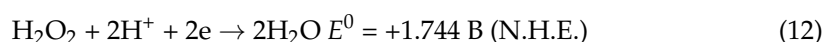
As is known, the O_2 reduction is a multi-stage process, with one of them being the formation of H_2O_2 [70,71]. In acidic solutions, this reaction can take the following form (first stage) by the following net reaction:



Because the simultaneous participation of two electrons is unlikely, the reaction can be considered in the first stage:



In acidic solutions, the further fate of H_2O_2 may be related to the electrochemical reduction of hydrogen peroxide (second stage) by the following net reaction:



and/or its catalytic net decomposition:



It is known that the catalytic decomposition of hydrogen peroxide can proceed by a chain mechanism with the formation of OH^\bullet [71]. The influence of defects of the Pt surface significantly accelerates the process of decomposition on a smooth Pt surface, as shown by W. Spring in the XIX century.

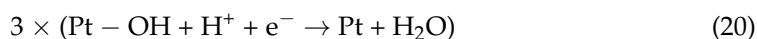
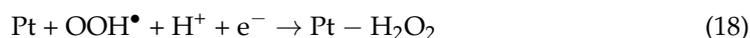
The addition of the first electron is the first stage of hydrogen peroxide reduction [70].



Currently, a number of researchers believe that the difficult oxygen reduction reaction (ORR) proceeds with the formation of an adsorbed radical OOH^\bullet [74–77], in agreement with the following reactions:



In a bifurcation mechanism, it is assumed that the adsorbed OOH^\bullet species is an intermediate that is capable of producing H_2O_2 or H_2O [78]. Therefore, the process of O_2 reduction may include either two or four electrons in an acidic media on Pt(111) at potential in the region of hydrogen adsorption [79]. A possibility of reduction of adsorbed OOH^\bullet to H_2O_2 followed by the catalytic decomposition of peroxide O_{ads} and OH has also been considered [80]. An even more complicated mechanism that occurs at low concentrations of oxygen in solutions has been proposed [81]:



Thus, the mechanism of oxygen reduction on Pt is presently disputable and not established. However, one may see that H_2O_2 is one of the key products produced in the course of ORR. The presence of hydrogen peroxide in a constant concentration in water depends significantly on pH of the solution. According to Schumb et al. [82], H_2O_2 is most stable in aqueous solutions at pH 4.0, which is close to the value of pH 3.85 in the studied electrolyte.

It is known [70–73] that the extent of oxidation of the Pt surface exerts a significant influence on the kinetics of the first (reaction 10) and second (reaction 12, 13) stage. The pre-oxidation of the electrode results in a decrease of the rate of O_2 reduction to H_2O_2 (reaction 10), as oxygen is mainly reduced at the sites that are free of oxides. For acidic solutions, it has been shown that the H_2O_2 yield on the reduced Pt surface increases by 70–90%. Under the conditions of our experiment, the concentration of dissolved oxygen is low (see Experimental). In this case, it can be expected that the oxygen reduction process should proceed under conditions of a latent limiting diffusion current. Therefore, in the conjugate reduction reaction of O_2 , as we assume, the process of its reduction is only completed at the stage of addition of two electrons. This is due to the fact that oxygen reduction products participate in rCO_2 oxidation and they are removed from the O_2 reduction reaction zone. The oxygen reduction process takes place under quasi-equilibrium conditions on the part of the Pt surface that is free from adsorbed rCO_2 .

Electrochemical and non-electrochemical reactions in the H_2O_2 -CO system on a Pt electrode were studied in 2M H_2SO_4 with cyclic voltammetry and on-line mass spectrometry [83]. It was found that the complete CO monolayer is chemically stable in the presence of dissolved H_2O_2 . However, H_2O_2 oxidizes adsorbed CO to CO_2 at lower potentials than those that are required for the electrochemical CO_{ads} oxidation when the Pt electrode is

partially covered by CO. It was observed that the complete CO monolayer on Pt inhibits the electrochemical reduction of H_2O_2 to H_2O in the CO-containing solution. It has been proposed [83] that the non-electrochemical hydrogen peroxide decomposition proceeds in the vacancies of the CO_{ads} adlayer. In studying the preparation of Pt deposits that are included in the Nafion films on glassy carbon, it was shown that hydrogen peroxide oxidizes chemisorbed CO on Pt. Up to 70% of CO_{ads} can be removed with peroxide, depending on the concentration of hydrogen peroxide [84]. The pre-ignition region of the peak oxidation of CO_{ads} in the region $E = 0.36\text{--}0.6$ V that is associated with the oxidation of CO on defect sites of Pt is discussed in the literature on the oxidation of CO_{ads} . The nature of the defect sites is not clear for this reaction and it is still being discussed [28]. A significant number of pcPt surface defects in the form of etching pits (Figure 1b–f) having a significant contribution to the total surface area of Pt, but not to the rCO_2 formation on Pt(111) can be a real source of active oxidant particles involved in oxidation in the vicinity of the defects of chemisorbed rCO_2 . Under our conditions, the total surface coverage of rCO_2 is equal to $\sim 0.7 \pm 0.05$ of the monolayer only. Therefore, there are many sites for the H_2O_2 formation. It was shown [85] that a negative surface charge inhibits the hydrogen peroxide reduction on Pt(111); this inhibition is not related to hydrogen adsorption and the OH_{ads} particle favors the reduction of hydrogen peroxide. It is known that Pt(111) is most catalytically active with respect to oxygen reduction [8].

Under our conditions, the amount of H_2O_2 on the electrode surface may be equal to $\sim 10^{-7}\text{--}10^{-8}$ M, which is commensurable with the amount of adsorbed rCO_2 . For the stage (12, 13), the presence of oxides on the Pt surface may cause an accelerating effect by also providing catalytic decomposition of hydrogen peroxide. Thus, the oxidized areas of the Pt surface may also be a source of the active oxidizer (reaction 13). Hydrogen peroxide is formed in the entire range of oxygen reduction potentials. For the reaction of O_2 reduction in acidic solutions, the change of the surface activity of a smooth Pt electrode under the influence of the anions adsorbed can be observed. Accordingly, it is known that the potential of the half-wave reduction of O_2 is shifted to the region to lower values of potentials in the following order of acids: $\text{HClO}_4 < \text{H}_2\text{SO}_4 < \text{HCl} < \text{HBr}$, i.e., as the specific adsorption of the anion increases [70]. This means that the half-wave potential of O_2 reduction should be located at a high value of the anode potential under our conditions in the H_2CO_3 solution in the absence of the specific adsorption of CO_3^{2-} , which is probably quite close to the half-wave potential in HClO_4 of the same concentration. For the reduction of O_2 under conditions that are close to stationary ones in the 0.5 M H_2SO_4 solution at positive potentials under oxidized electrode conditions, it was shown that the total reaction rate is determined by the rate of hydrogen peroxide formation. On the other hand, when the potential is shifted to the region of lower values on the reduced Pt electrode, the rate of H_2O_2 reduction determines the overall reaction rate [70] and then OH^\bullet will be able to form (reaction 14).

The next question is what are other species that can be a source of hydroxyl radicals in the system under consideration? According to [86], after the active bubbling of air through water after collapsing microbubbles in the absence of dynamic stimulus, the authors found the presence of OH^\bullet in the solution volume. The electron paramagnetic resonance method was used with 5,5-dimethyl-1-pyrroline-N-oxide (DMPO) as a spin trap reagent in order to identify the radicals. The formation of reactive oxygen species was observed when water was irradiated with visible, infrared light and with a cavitation collapse [87]. It was shown that additional free energy can be accumulated in the form of surface tension in air nanobubbles (bubble stabilized by ions) [88,89]. According to [90], all the values of the ζ -potential were negative, and absolute values were in the range between 34–45 mV (O_2), 17–20 mV (air), 29–35 mV (N_2), 20–27 mV (CO_2), and 11–22 mV (Xe). Therefore, it is possible to expect the electrophoresis phenomenon of bubbles to the parts of the Pt surface. The potential fluctuations that are observed by us when registering transients (Figure 10a–c) can qualitatively reflect the picture of interaction of Pt with dissolved CO_2 and O_2 bubbles, during which local resistances of surface areas can change [22–24]. It becomes obvious that, in the future, it is necessary to consider the dynamics of the behavior

of CO₂ bubbles in the electrolyte under consideration in accordance with the methods that were proposed by Bunkin et al. [30,37,88,89]. Finally, when obtaining ultra-pure water (see Methods), it was irradiated with ultraviolet light. This could also lead to the formation of reactive oxygen forms in water, in particular, the formation of OH•. The question as to what extent these factors can affect the oxidation of rCO₂ in our conditions will require a separate research.

When considering the mechanisms of rCO₂ oxidation on the surface of the (pc)Pt electrode, it is necessary to identify particles that may be considered as candidates for the role of an oxidant under open-circuit and electrochemical conditions. By using electrochemical and catalytic methods, it is a serious problem to determine a number of the particles that are capable of acting as an oxidizer for rCO₂, because the lifetime of such particles is small, and the time of the product and chemical bond formation in molecules is equal to ~10⁻¹³–10⁻¹⁴ s in the volume of solutions [91]. Voltammetry experiments in the presence of spin traps on Pt and C electrodes allowed for one to detect OH• during the H₂O₂ oxidation. Under these conditions, the hydroperoxide radical OOH• was not detected [92]. These results identify the hydroxyl radical as a key species responsible for the oxidation of H₂O₂ in both carbon and platinum electrode substrates. At present, interactions with OH_{ads} particles, in particular, OH⁻ anions and/or OH• radicals, are considered during the oxidation of CO_{ads} in an aqueous medium, as well as with adsorbed atomic O if the reaction proceeds in the gas phase [32]. Formally, the role of the oxidant in an aqueous medium can be played by dissolved O₂, which is present in the soluble state mainly in the molecular form in the concentration that was estimated by us (see the Methods section), adsorbed particles as atomic oxygen O, OH⁻ anion, radicals, such as O₂⁻ or OH• and H₂O itself. We compared the anion OH_{ads} (aOH) and radical OH (rOH) as potential oxidizing particles in the rCO₂ oxidation reaction using DFT calculations.

We have attempted to identify the possible candidates for the role of oxidants using the DFT calculation of the simplest magic platinum cluster Pt₁₃ [41–47]. It is obvious that this simplest Pt model has a number of disadvantages, which make this cluster a very rough approximation of the actual experimental system. One of the disadvantages of the model, for example, is the lack of a rigid cluster framework and its very small size. However, it is known that the surface platinum atoms have fairly high mobility. On the other hand, it is known that CO_{ads} at the surface of Pt exists in the form of two-dimensional islands that represent surface clusters [93,94], whereas the reaction of CO oxidation occurs in agreement with the Langmuir–Hinshelwood mechanism at the border of these islands. Consequently, the oxidation process takes place in an extremely narrow reaction zone. Therefore, the choice of cluster models for an analysis of the mechanism of rCO₂ oxidation on Pt may be reasonable. We only used this model to obtain an estimate of the effects and only in the first approximation. This task needs to be solved in the future for more complex systems that require more serious computational resources.

Accordingly, to analyze the electrostatic component with the goal of determining the probability of interaction of the linear form of CO_{ads} with OH_{ads} species on Pt, DFT calculations were performed and the charge distribution on the CO_{ads} molecules with adsorbed OH⁻ and OH• on the 13-atom Pt cluster were determined as a first step; Table 2 presents the results.

It can be seen that the charge separation is observed on Pt₁₃ and the adsorbed substrates in the systems under consideration. It can be seen from these data (Table 2) that the natural charge on Pt₁₃ acquires an increasingly negative value as the number of adsorbed molecules CO_{ads} on Pt increases. The composition of rCO₂ is represented by CO_{ads}. From electrochemical data, it is known that the potential of zero total charge will be shifted to the region of higher anode potential values during the adsorption of CO on the Pt surface and may even be unattainable under electrochemical conditions due to the oxidation of chemisorbed CO_{ads} on Pt [10,11,13,95]. Under electrochemical conditions, the adsorption of cations will prevail in terms of electrostatic interaction, and anions will be removed to the outer layer of the DEL on the Pt surface covered rCO₂.

Table 2. Natural charges in systems $\text{Pt}_{13}(\text{CO})_n$, $\text{rOH-Pt}_{13}(\text{CO})_n$ and $\text{aOH-Pt}_{13}(\text{CO})_n$, $\text{rOH-Pt}_{13}(\text{COH})$, $\text{aOH-Pt}_{13}(\text{COH})$, $\text{rOH-Pt}_{13}(\text{COOH})$, $\text{aOH-Pt}_{13}(\text{COOH})$.

Structure	Pt ₁₃	CO	OH
Pt ₁₃ -CO	−0.03	0.03	−
Pt ₁₃ -(CO) ₂	−0.02	0.01	−
Pt ₁₃ -(CO) ₃	−0.12	0.04	−
Pt ₁₃ -(CO) ₄	−0.20	0.05	−
r-OH-Pt ₁₃ -CO	0.38	0.03	−0.41
r-OH-Pt ₁₃ -(CO) ₂	0.36	0.02	−0.40
r-OH-Pt ₁₃ -(CO) ₃	0.25	0.05	−0.40
r-OH-Pt ₁₃ -(CO) ₄	0.18	0.05	−0.38
a-OH-Pt ₁₃ -CO	−0.43	−0.07	−0.50
a-OH-Pt ₁₃ -(CO) ₂	−0.38	−0.06	−0.50
a-OH-Pt ₁₃ -(CO) ₃	−0.33	−0.06	−0.49
a-OH-Pt ₁₃ -(CO) ₄	−0.35	−0.04	−0.49
Structure	Pt	(Pt ₃) rCOH	OH
rOH-Pt ₁₃ -(rCOH)	0.67	−0.214	−0.457
aOH-Pt ₁₃ -(rCOH),	−0.257	−0.747	−0.483
Structure	Pt	(Pt ₁)rCOOH	OH
rOH-Pt ₁₃ -(rCOOH)	0.561	−0.147	−0.415
aOH-Pt ₁₃ -(rCOOH),	0.005	−0.28	−0.484

A different pattern is observed in the presence of an OH^\bullet radical on the Pt surface (Table 2). In this case, Pt_{13} carries a significant positive surface charge, while the adsorbed OH^\bullet species has a negative charge. In terms of electrostatic interaction, such a system can be expected to be more stable. It can also be expected that, in the presence of adsorbed OH^\bullet , the probability of the interaction of CO_{ads} with OH^\bullet will be increased. The CO_{ads} molecule remains practically as an electroneutral particle for all types of systems under consideration with a different number of CO molecules (Table 2), and it does not fundamentally affect the charge distribution on Pt and OH_{ads} . From the electrostatic point of view, it can also be seen that in the systems $\text{rOH-Pt}_{13}(\text{COH})$, $\text{aOH-Pt}_{13}(\text{COH})$, $\text{rOH-Pt}_{13}(\text{COOH})$, and $\text{aOH-Pt}_{13}(\text{COOH})$, complexes are most stable in the presence of the adsorbed OH^\bullet species. The DFT calculations have confirmed that Pt_3COH is the most preferred form of bonding between the adsorbed COH radical and Pt surface. The Pt_3COH complex is significantly more stable than the PtCOH complex by ~ 30 kcal/mol.

In the specified experimental conditions, a part of the (pc)Pt surface sites is free of rCO_2 (Figure 3a,b). Let us assume that these are mainly the surface sites with the orientation Pt(111) according to Figures 1 and 3b (the factor of roughness is small, see the Methods section). Subsequently, in this case, the potential of the zero total charge for these sites at the surface can be considered separately, while referring it to Pt(111). The application of this approach is reasonably considered in the publication [96]. The potential of the zero total charge (p.z.t.c.) on Pt(111) in a solution of HClO_4 at pH 3.1 is 0.46 V (R. H. E.), both in the presence and absence of CO_2 in the solution [97]. The same value corresponds to the potential of zero free charge. When the pH value changes from 1.98 to 3.1 (ΔpH is equal to 1.12), the change in the potential of the zero full charge is about 40 mV, then in our case (pH 3.85) compared to pH 3.1 (ΔpH is equal to 0.75) [97] the change in the potential of the zero full charge will be less than 40 mV. Therefore, under the conditions of the above measurements, the potential of the zero total charge will be in the range $E = 0.46\text{--}0.5$ V (0.48 ± 0.02 V). Subsequently, at potentials >0.48 V, the adsorption of anions (OH^- , CO_3^{2-}) on Pt(111) will begin to increase. According to the data that are presented in Figures 3a, 7a and 8a, the rCO_2 oxidation begins in the region of 0.45–0.48 V and it clearly increases at a potential >0.5 V, i.e., in the vicinity of the Pt(111) p.z.t.c., and continues at more anodic E values. This allowed for us to proceed to the analysis to identify the

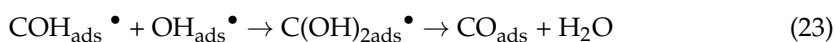
possible candidates for the role of oxidants for $r\text{CO}_2$, while taking into account the possible participation of OH-particles adsorbed on the surface of the (pc)Pt electrode.

We assume that the particles exist in their main unexcited states under our experimental conditions on the surface of the Pt electrode. This assumption may be supported, for example, by the fact that $\sim 5\text{--}6$ eV is required for the conversion of the CO molecules to an excited state, which is unlikely under the conditions of our measurements. The diamagnetic diatomic moieties under consideration will have the following configurations: $\text{CO}(X^1\Sigma)$, $\text{CO}_2(X^1\Sigma)$, $\text{OH}^\bullet(X^2\Pi)$, $\text{OH}^-(X^1\Sigma^+)$, and $\text{O}_2(X^3\Sigma^-_g)$; whereas, the monoatomic species can be represented as $\text{O}(X^3P)$, $\text{H}(^2S)$, and triatomic molecule—as $\text{H}_2\text{O}(X^1A_1)$ [98].

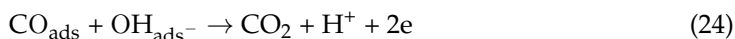
Under open-circuit conditions, in the case of oxidation, a periodic process is observed (Figure 10b). In gas-phase catalysis, the mechanism of alternating reduction–surface oxidation (the Mars–Van Krevelen mechanism) is known. If the hydrogen concentration is excessive and the surface coverage of Pt with oxygen is low, then hydrogen in the atomic form is involved in the reaction with adsorbed oxygen. The formation of water is preceded by the intermediate formation of adsorbed OH groups, which, upon further interaction with hydrogen, turn into water in the singlet state (X^1A_1). At the experimental conditions under consideration, such interactions may lead to periodic local changes of the local resistances on the electrode surface sections, leading to oscillations recorded in the current–voltage dependences, which is observed in Figure 10 [22–24]. The following reactions involving the H_{ad} and CO_{ad} adsorbed species are possible in the region of hydrogen adsorption potentials and reduction of O_2 for the case of an open circuit:



Under open-circuit conditions, the following surface reactions for adsorbed particles involving intermediates may be assumed:



this reaction (23) is followed by reaction (22). Formally, it is possible to record the oxidation reaction of CO_{ads} with the participation of an adsorbed particle OH^- :



However, the transfer of two electrons in one elementary act in an open circuit is less likely in reaction 24. This may indicate the course of the reaction (13), rather than the anodic oxidation of CO_{ads} via the interaction with the OH_{ads} anion. The possible electrostatic repulsion of OH^- anions from the part of the surface of the (pc)Pt electrode with $r\text{CO}_2$, as was shown above, reduces the probability of the interaction of the CO_{ads} species with the adsorbed OH^- anion. Therefore, we assume that, under open-circuit conditions, OH_{ads}^- cannot be considered to be an oxidant in the direct oxidation reaction of $r\text{CO}_2$.

Thus, based on the above reasoning, we assume that the oxidation of H_{ad} and $r\text{CO}_2$ preferably proceeds under open-circuit conditions by a radical mechanism, which is a rapid process. The recovery of dissolved molecular oxygen is the slow stage. The quantum chemical calculations were carried out to confirm or reject our working hypothesis. The two-stage reaction 22 is the key stage of the $r\text{CO}_2$ oxidation reaction (reaction 23 proceeds via CO_{ads} formation followed by reaction 22).

The quantum-chemical calculations (the potential energy surface, PES) of the reaction 22 carried out for the case of the spontaneous reaction in isobaric-isothermal conditions demonstrated that the obtained energy parameters of the process (Tables 3 and 4) with OH^\bullet are more optimal for reaction 22 than with OH^- for the same reaction. The quantum-chemical calculations shown in Table 3 were not performed on the two adjacent Pt atoms (O-Pt-Pt-O), but on two Pt atoms with another Pt atom in between (O-Pt-Pt-Pt-O). This was connected with the steric hindrances.

Table 3. The results of quantum-chemical calculations of the potential energy surface (PES) for reaction 22 with radical OH (rOH) and OH_{ads} (aOH) in the gas phase.

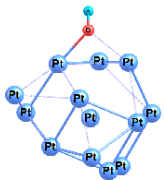
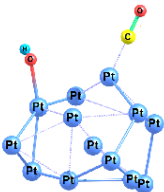
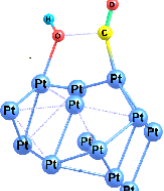
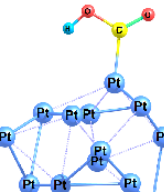
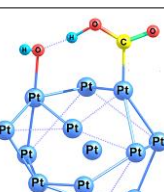
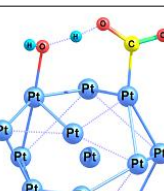
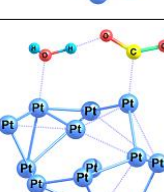
Number of the Structure	Structure	ΔE , kcal/mol rOH	ΔG , kcal/mol rOH	ΔE , kcal/mol aOH	ΔG , kcal/mol aOH
0		0.0	0.0	0.0	0.0
1		−40.9	−28.0	−41.3	−29.0
1-ts		−25.1	−12.1	−20.9	−7.6
2-1		−35.7	−22.1	−44.2	−30.7
2-2		−52.5	−39.9	−44.4	−30.9
2-ts		−52.5	−39.6	−42.9	−31.4
3		−54.5	−40.3	−44.0	−30.6

Table 4. The results of quantum-chemical calculations of the PES for reaction 22 with rOH and aOH in aqua media.

Number of the Structure	ΔE , kcal/mol rOH	ΔG , kcal/mol rOH	ΔE , kcal/mol aOH	ΔG , kcal/mol aOH
0	0.0	0.0	0.0	0.0
1	−44.3	−31.8	−40.5	−27.6
1-ts	−26.5	−13.0	−21.7	−7.6
2-1	−41.7	−28.0	−36.4	−22.7
2-2	−41.4	−28.0	−37.1	−24.3
2-ts	−41.5	−28.3	−34.0	−20.7
3	−43.4	−29.3	−36.8	−25.1

It can be seen (Tables 3 and 4) that, in both the gas phase and aqueous medium, the reaction 22 with the participation of OH^\bullet is more preferable than with the participation of OH^- , since it is less energy-intensive (column ΔG). The energy gain is $\sim 5\text{--}10$ kcal/mol ($\sim 0.25\text{--}0.5$ eV). The obtained ΔG values (Table 3) correlate well with the experimental chemisorption energies of CO, where the binding energy of CO_{ads} with Pt (100) from the gas phase at $\theta > 0.5$ varies within 26.5 ± 2.5 kcal/mol [99]. For comparison, the quantum-chemical calculations were performed for the reaction



It turned out that, in this case, the reaction is difficult to proceed for energy reasons, because the values ΔG are positive at all stages of the process.

Thus, the preliminary and tentative quantum-chemical calculations that were carried out on Pt_{13} as a first step of theoretical solutions of rCO_2 oxidation confirm our assumptions regarding the radical mechanism of the oxidation process of rCO_2 on Pt under open-circuit conditions.

Under electrochemical conditions, according to Noguchi [100], the number of adsorbed OH_{ads} particles on the Pt surface is small in the region of DES potentials. The H_2O adsorption on the surface of the Pt electrode was studied in situ by SFR in the 0.1 M HClO_4 solution in a wide range of potentials (0.05–1.3 V (R. H. E.)) [100]. The authors observed the formation of OH_{ads} species on Pt. Their concentration varied markedly, depending on the imposed external potential. The SFG dependences exhibited a U-shape in the region of potentials 0.05–0.8 V. The minimum intensity of the SFG signal was observed in the region of the DEL potentials (~ 0.4 V), the maximum value of the SFG signal was reached at ~ 0.8 V, whereas a decrease in the intensity of the SFG signal was observed at higher potential values. The considered region of oxidation potentials of OH_{ads} on Pt [100] corresponds to the oxidation region of rCO_2 , i.e., at potentials that are much more positive than the potentials of the adsorption–desorption region of H_{ad} . Glucose oxidation on Pt electrodes in acidic solutions was studied under electrochemical conditions [101]. The oxidation rate of organic molecules at potentials < 0.7 V (R. H. E.) was determined by the interaction with OH_{ads} formed by the oxidation reaction of OH^- to OH_{ads} . On Au electrodes in alkaline solutions, the adsorption of OH^- can be accompanied by the formation of OH^\bullet [102]. When discussing the mechanisms of the electrochemical oxidation of rCO_2 , OH^\bullet is considered to be an oxidant [67–69].

The reaction (23) in the potentials region of the H_{ad} adsorption is possible for the H_{ad} oxidation under electrochemical conditions of measurements (Figures 1a and 5a). However, obviously, the greatest contribution will be made by the other reaction:



because the affinity of the proton to the electron is maximal, the surface concentration of electrons on Pt is much higher than the concentration of $\text{OH}_{\text{ads}}^\bullet$ radicals, and the electron is the fastest active particle.

It should be noted that the oxidation of aOH to rOH in the volume of an aqueous solution under normal conditions is thermodynamically unprofitable [103] and at $T = 298.15 \text{ K}$ is $+110$ – $+123 \text{ kcal/mol}$. The reason for this is the high hydration energy of aOH. At the same time, the hydration energy of rOH is negligible, i.e., it is a very weakly hydrated particle [103]. The dehydration energy of the adsorbed OH^- is $\sim +40 \text{ kcal/mol}$, according to our preliminary calculations for Pt_{13} . There is a hope that the oxidation of aOH to rOH is still possible on Pt according to the reaction:



The formation of $\text{OH}_{\text{ads}}^\bullet$ under electrochemical conditions is also possible on the Pt surface by chain reactions (13) and (14).

The quantum-chemical calculations showed that, in the considered model complexes (Table 2), the vertical ionization potentials of OH_{ads} are equal to: in aOH- Pt_{13} 3.40 eV (78.3 kcal/mol); aOH- $\text{Pt}_{13}(\text{CO})_1$ 3.55 eV (81.80 kcal/mol); aOH- $\text{Pt}_{13}(\text{CO})_2$ 3.69 eV (85.01 kcal/mol); aOH- $\text{Pt}_{13}(\text{CO})_3$ 3.83 eV (88.23 kcal/mol); and, aOH- $\text{Pt}_{13}(\text{CO})_4$ 4.09 eV (94.21 kcal/mol). Taking the reference hydration energy of OH^- species ($-109.975 \text{ kcal/mol}$) into account, we obtained the following ionization potentials of the OH_{ads}^- oxidation ΔG : aOH- Pt_{13} -1.375 eV (-31.675 kcal/mol); aOH- $\text{Pt}_{13}(\text{CO})_1$ -1.223 eV (-28.175 kcal/mol); aOH- $\text{Pt}_{13}(\text{CO})_2$ -1.084 eV (-24.969 kcal/mol); aOH- $\text{Pt}_{13}(\text{CO})_3$ -0.944 eV (-21.745 kcal/mol); and, aOH- $\text{Pt}_{13}(\text{CO})_4$ -0.684 eV (-15.765 kcal/mol). It follows from the obtained data that, as the number of CO_{ads} increases, the oxidation potential of OH_{ads}^- in accordance with the reaction (26) decreases. Similar calculations were also performed while taking into account the influence of the presence of water in the system on the Pt_{13} cluster. According to the calculated data for Pt_{13} , the ΔG values for the oxidation of adsorbed OH^- demonstrate a linear trend in units of V presented as the E , N_{CO} dependence (Figure 11, curves 1,2), where N_{CO} is the number of CO_{ads} molecules in the linear form on the Pt_{13} cluster. It is clearly seen that, when extrapolated to the formal value $n = 5$ – 10 , the oxidation potential is located in the vicinity of 0.5 eV, which correlates with experimental data on the oxidation of rCO_2 on (pc)Pt under electrochemical conditions in potentiodynamic and galvanostatic measurements (Figures 3a and 7a).

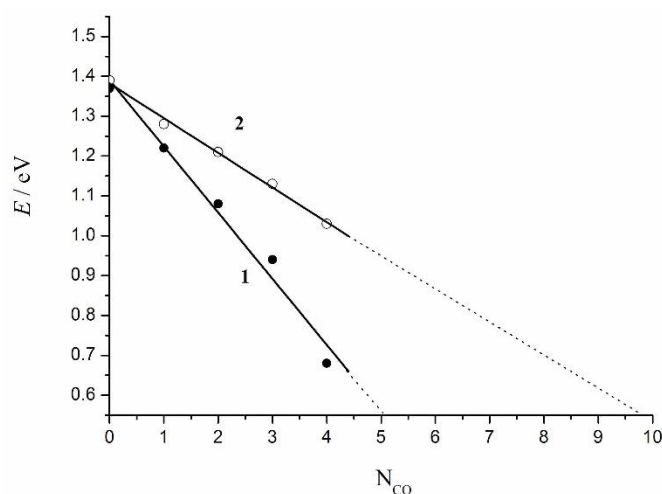
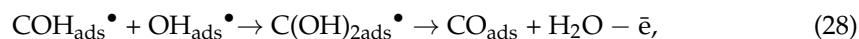


Figure 11. Potentials of the OH_{ads}^- anion oxidation, depending the number of CO on the cluster Pt_{13} (1) and while taking the influence of water at solutions (2) into account.

Under electrochemical conditions of the measurements, the $r\text{CO}_2$ oxidation will proceed by reactions 22 and 23 as follows:



this reaction is followed by reaction (27).

The electrochemical mechanism (reactions 26, 27, 28) of $r\text{CO}_2$ oxidation can be based on the mechanism proposed in the literature and presented in the form of a ladder-matrix scheme [28].

When moving from the pre-ignition region to the region of higher anode potential values under electrochemical conditions, the slopes change on the Tafel (Figure 5) dependences and on the dependences at Figure 9a–c, because the deceleration of the oxidation process takes place. We assume that the slope 0.099 V of Tafel dependences is defined by the electrochemical stage of the electron transfer according to the reaction 26, followed by a rapid step according to the reaction 27 and/or 28 in the pre-ignition region. This process takes place in the vicinity of the islands of the platinum surface that is covered with chemisorbed $r\text{CO}_2$. As already noted above, there were no changes in the frequency of oscillations of the current and potential values (Figure 10). Consequently, no new oxidizing particles were detected in the near-electrode layer of Pt, the resulting intermediates do not pass into the volume of the solution, which is consistent with spectroscopic data. Therefore, we can also assume that no change of the mechanism of the $r\text{CO}_2$ oxidation reaction occurs upon passing the potential >0.6 V. As to the change of the slope on the Tafel dependences (Figure 6) and anamorphoses (Figure 9a–c), it results from the new limiting surface reactions: $\text{H}_2\text{O} \rightarrow \text{OH}_{\text{ads}} + \text{H}^+ + \bar{e}$ occurring in the presence of chemisorption forms of $r\text{CO}_2$ with the subsequent formation of radicals $\text{OH}_{\text{ads}}^\bullet$ according to reaction 26 at the potentials over 0.6 V, which can lead to a noticeable deceleration of the oxidation process of $r\text{CO}_2$. This conclusion is consistent with the conclusion that was drawn earlier [57]. Under the considered electrochemical conditions and in open-circuit conditions, H_2O acts as a precursor in the formation of the active form of OH_{ad} on the Pt surface and it is not as an oxidizer.

It is known that, depending on the chosen basis set in quantum-chemical model calculations (the density functional theory), the electron can be either delocalized or localized [104] on the particle. Therefore, the results of the calculations may differ and, in the future, when considering quantum-chemical models that describe our system, it will be necessary to take this factor into account.

5. Conclusions

The electrochemical data that were obtained by us for a saturated aqueous solution of $\text{CO}_2 + \text{H}_2\text{CO}_3$ are in good agreement with the results obtained earlier for electrolytes with low pH values in solutions that do not contain specifically adsorbed anions on the surface of (pc)Pt. The measurements revealed a correlation between the oxidation of $r\text{CO}_2$ under electrochemical and open-circuit conditions of measurements. The correspondence in the energy parameters of the oxidation process of $r\text{CO}_2$ under open-circuit conditions and electrochemical conditions is shown. Periodic oscillations are revealed at the oxidation of H_{ad} and $r\text{CO}_2$ on (pc)Pt. The possibility of the formation of a radical particle as an intermediate due to the radical oxidation mechanism of $r\text{CO}_2$ is considered in the framework of our consideration. Preliminary quantum-chemical calculations on Pt_{13} confirm this assumption. OH^\bullet species was chosen as the most likely candidate for the role of the oxidant. The optimal PES for the main reaction $\text{CO}_{\text{ads}} + \text{OH}_{\text{ads}}^\bullet \rightarrow \text{COOH}_{\text{ads}}^\bullet + \text{OH}_{\text{ads}}^\bullet \rightarrow \text{CO}_2 + \text{H}_2\text{O}$ is revealed. It is shown that radical particles can be involved in a radical mechanism, being a fast stage of reactions. The ionization potentials of OH_{ads}^- oxidation are revealed, which confirms the conclusion regarding the radical mechanism of the $r\text{CO}_2$ oxidation. The precursor of $\text{OH}_{\text{ads}}^\bullet$ radicals in electrochemical conditions can be OH_{ads}^- at potentials

in the vicinity of 0.5–0.6 V, and also H₂O at more anodic values of potentials. In this case, neither OH_{ads}[−] nor H₂O are oxidants and they do not participate in the elementary act of the reaction. In open-circuit conditions, the precursor is mainly hydrogen peroxide, which is formed from dissolved oxygen during its reduction. It is assumed that under electrochemical conditions as a slow stage of the rCO₂ oxidation is the oxidation of OH_{ads}[−] with a formation of OH_{ads}[•]. As a slow stage in open-circuit conditions, it is proposed to consider the accumulation of an oxidant during the reduction of molecular oxygen on the surface of Pt. Under our conditions, the accumulation of the oxidant is based on the periodic nature of the process.

It is important to note that the electrochemical processes of CO₂ reduction and rCO₂ oxidation should be considered to be conjunct processes occurring via similar transitions states and intermediates [105–108]. Therefore, the solution of the problem of rCO₂ oxidation may help to develop efficient ways for the CO₂ electrochemical reduction. The method of the thorough purification of the electrolyte from dissolved oxygen impurities using ultra-pure He allows us to more accurately control the impurities of the dissolved oxygen and analyze the kinetics of the oxidation on smooth electrodes. The proposed method will allow for us to create sensors for small concentrations of the dissolved oxygen. On the other hand, the use of small H₂O₂ additives in the fuels of fuel cells may favorably affect the solution of the first problem of the fuel cell—the poisoning of the catalyst surface with fuel chemisorption products.

Author Contributions: A.V.S.—Methodology, Investigation; Writing—original draft preparation, A.F.G.—Visualization, Formal analysis, M.N.M.—Software, Data curation, Validation, L.M.K.—Conceptualization, Supervision, Writing—Editing. All authors have read and agreed to the published version of the manuscript.

Funding: The reported study was funded in the part related to the materials preparation by Russian Science Foundation, project number 20-63-46013, and in the part related to materials electrochemical studies by the Ministry of Science and Higher Education of the Russian Federation in the framework of Increase Competitiveness Program of NUST «MISiS» (No. K1–2015–045).

Institutional Review Board Statement: Not applicable.

Informed Consent Statement: Not applicable.

Data Availability Statement: Not applicable.

Acknowledgments: The authors thank K. Kalmykov (Chemistry Department of Moscow State University) for SEM measurements, V. Kuzmin (MIREA) and S. Vasiliev (Chemistry Department of Moscow State University) for valuable comments and discussion.

Conflicts of Interest: There is no conflict to declare.

References

1. Hori, Y. *Electrochemical CO₂ Reduction on Metal Electrodes. Modern Aspects of Electrochemistry*; Springer Inc.: New York, NY, USA, 2008; pp. 89–189.
2. Gómez-Marín, A.M.; Feliu, J.M. Oxygen reduction at platinum electrodes: The interplay between surface and surroundings properties. *Curr. Opin. Electrochem.* **2018**, *9*, 166–172. [[CrossRef](#)]
3. Briega-Martos, V.; Herrero, E.; Feliu, J.M. Pt(hkl) surface charge and reactivity. *Curr. Opin. Electrochem.* **2019**, *17*, 97–105. [[CrossRef](#)]
4. Malara, A.; Leonardi, S.G.; Bonavita, A.; Fazio, E.; Stelitano, S.; Neri, G.; Neri, F.; Santangelo, S. Origin of the different behavior of some platinum decorated nanocarbons towards the electrochemical oxidation of hydrogen peroxide. *Mater. Chem. Phys.* **2016**, *184*, 269–278. [[CrossRef](#)]
5. Chen, Y.; Li, Q.; Jiang, H.; Wang, X. Pt modified carbon fiber microelectrode for electrochemically catalytic reduction of hydrogen peroxide and its application in living cell H₂O₂ detection. *J. Electroanal. Chem.* **2016**, *781*, 233–237. [[CrossRef](#)]
6. Zheng, Y.; Chen, W.; Zuo, X.-Q.; Cai, J.; Chen, Y.-X. The kinetics of the oxidation and reduction of H₂O₂ at a Pt electrode: A differential electrochemical mass spectrometric study. *Electrochem. Commun.* **2016**, *73*, 38–41. [[CrossRef](#)]
7. Sitta, E.; Da Silva, K.N.; Feliu, J.M. Hydrogen Peroxide Oxidation/Reduction Reaction on Platinum Surfaces. In *Encyclopedia of Interfacial Chemistry: Surface Science and Electrochemistry*; Wandelt, K., Ed.; Elsevier Inc.: Amsterdam, The Netherlands, 2018; Volume 5.2, pp. 682–689.

8. Gómez-Marín, A.M.; Feliu, J.M. Oxygen Reduction on Platinum Single Crystal Electrodes. In *Encyclopedia of Interfacial Chemistry: Surface Science Electrochemistry*; Wandelt, K., Ed.; Elsevier Inc.: Amsterdam, The Netherlands, 2018; Volume 5.2, pp. 820–830.
9. Conway, B.E. Some theoretical problems in electrocatalysis with charge transfer. *J. Molec. Catal.* **1989**, *54*, 353–369. [[CrossRef](#)]
10. Podlovchenko, B.I.; Gladysheva, T.D. Adsorption and electrooxidation of carbon monoxide on platinized platinum at low anodic potentials. *Russ. J. Electrochem.* **1998**, *34*, 256–262.
11. Smolin, A.V.; Podlovchenko, B.I. Electrochemical behavior of carbon monoxide on electrolytic deposits of palladium in sulfuric acid solutions. *Russ. J. Electrochem.* **1998**, *34*, 263–270.
12. Podlovchenko, B.I.; Gladysheva, T.D.; Smolin, A.V. Transients of current at the adsorption of carbon monoxide on platinum and palladium electrodes. *Mendeleev Commun.* **1999**, *3*, 97–99. [[CrossRef](#)]
13. Podlovchenko, B.I. Interrelation between transients of current and open-circuit potential during adsorption of neutral particles. *Russ. J. Electrochem.* **2000**, *36*, 821–824.
14. Frumkin, A.N.; Petrii, O.A.; Damaskin, B.B. Potentials of zero charge. In *Comprehensive Treatise of Electrochemistry*; Bocris, J.O.M., Conway, B.E., Yeager, E., Eds.; Plenum Press: New York, NY, USA; London, UK, 1980; Volume 1, pp. 221–289.
15. Frumkin, A.N.; Petrii, O.A. The Dependence of Free Surface Energy of Platinum Electrode on Solution Potential and Composition. *Dokl. Akad. Nauk Sssr* **1971**, *196*, 1387–1390.
16. Manzhos, R.A.; Podlovchenko, B.I.; Maksimov, Y.M. Interaction of HCO-substances with adsorbed oxygen on platinum electrodes open-circuit transient reactions of HCOOH and CO. *Electrochim. Acta* **2005**, *50*, 4807–4813.
17. Manzhos, R.A.; Podlovchenko, B.I.; Maksimov, Y.M. Kinetics and mechanism of interaction between methanol and adsorbed oxygen on a smooth polycrystalline platinum electrode: Transients of the open-circuit potential. *Russ. J. Electrochem.* **2006**, *42*, 1061–1066.
18. Manzhos, R.A.; Podlovchenko, B.I.; Maksimov, Y.M. Special features of methanol interaction with adsorbed oxygen at platinized platinum electrode: Transients of the open-circuit potential. *Russ. J. Electrochem.* **2007**, *43*, 1268–1272. [[CrossRef](#)]
19. Podlovchenko, B.I.; Smolin, A.V.; Maksimov, Y.M. Formaldehyde interaction with adsorbed oxygen on open-circuit platinum electrodes in aqueous sulfuric acid solutions. *Russ. J. Electrochem.* **2009**, *45*, 246–251.
20. Smolin, A.V.; Podlovchenko, B.I. The Effect of Hydrocarbon Chain Length in Normal Aliphatic Alcohols on Their Reaction with Oxygen Adsorbed on Polycrystalline Platinum Electrode. *Russ. J. Electrochem.* **2010**, *46*, 367–373. [[CrossRef](#)]
21. Sakong, S.; Gross, A. Methanol Oxidation on Pt(111) from First-Principles in Heterogeneous and Electrocatalysis. *Electrocatalysis* **2017**, *8*, 577–586. [[CrossRef](#)]
22. Malkhandi, S.; Bauer, P.R.; Bonnefont, A.; Krischer, K. Mechanistic aspects of oscillations during CO electrooxidation on Pt in the presence of anions: Experiments and simulations. *Catal. Today* **2013**, *202*, 144–153. [[CrossRef](#)]
23. Orlik, M. *Self-Organization in Electrochemical Systems I-II*; Springer: Berlin/Heidelberg, Germany, 2012.
24. Machado, E.G.; Varela, H. Kinetic Instabilities in Electrocatalysis. In *Encyclopedia of Interfacial Chemistry: Surface Science and Electrochemistry*; Wandelt, K., Ed.; Elsevier Inc.: Amsterdam, The Netherlands, 2018; Volume 5.2, pp. 701–718.
25. Makeev, A.G.; Slinko, M.M.; Luss, D. Mathematical modeling of oscillating CO oxidation on Pt-group metals at near atmospheric pressure: Activity of metallic and oxidized surfaces. *Appl. Catal. A Gen.* **2019**, *571*, 127–136. [[CrossRef](#)]
26. Kim, M.; Bertram, M.; Pollmann, M.; Von Oertzen, A.; Mikhailov, A.S.; Rotermund, H.H.; Ertl, G. Controlling chemical turbulence by global delayed feedback: Pattern formation in catalytic CO oxidation on Pt(110). *Science* **2001**, *292*, 1357–1360. [[CrossRef](#)] [[PubMed](#)]
27. Kuzmin, V.I.; Tytik, D.L.; Gadzaov, A.F.; Abaturov, M.A.; Belashchenko, S.A.; Busev, D.K.; Kasatkin, V.E.; Smolin, A.V.; Tsetlin, V.V. *Discreteness and Continuity in the Properties of Physical-Chemical Systems*; Kuzmin, V.I., Tytik, D.L., Gadzaov, A.F., Eds.; FIZMATLIT: Moscow, Russia, 2014; p. 176. Available online: https://www.rfbr.ru/rffi/ru/books/o_1915369 (accessed on 31 December 2020).
28. Petrii, O.A. The progress in understanding the mechanisms of methanol and formic acid electrooxidation on platinum group metals (Review). *Russ. J. Electrochem.* **2019**, *55*, 1–33. [[CrossRef](#)]
29. Camara, G.A.; Iwasita, T. Parallel pathways of ethanol oxidation: The effect of ethanol concentration. *J. Electroanal. Chem.* **2005**, *578*, 315–321. [[CrossRef](#)]
30. Bunkin, N.F.; Ninham, B.W.; Babenko, V.A.; Suyazov, N.V.; Sychev, A.A. Role of Dissolved Gas in Optical Breakdown of Water: Differences between Effects Due to Helium and Other Gases. *J. Phys. Chem. B* **2010**, *114*, 7743–7752. [[CrossRef](#)] [[PubMed](#)]
31. Giner, J. Electrochemical reduction of CO₂ on platinum electrodes in acid solutions. *Electrochim. Acta* **1963**, *8*, 857–865. [[CrossRef](#)]
32. Breiter, M.W. On the nature of reduced carbon dioxide. *Electrochim. Acta* **1967**, *12*, 1213–1218. [[CrossRef](#)]
33. Vassiliev, Y.B.; Bagotzky, V.S.; Osetrova, N.V.; Mikhailova, A.A. Electroreduction of carbon dioxide part iii. adsorption and reduction of CO₂ on platinum metals. *J. Electroanal. Chem. Interfacial Electrochem.* **1985**, *189*, 311–324. [[CrossRef](#)]
34. Łukaszewski, M.; Siwek, H.; Czerwiński, A. Electroreduction of carbon dioxide on platinum group metals and alloys—A review. *J. Solid. State Electrochem.* **2009**, *13*, 813–827. [[CrossRef](#)]
35. Podlovchenko, B.I.; Stenin, V.F.; Ekibaeva, A.A. On the influence of the solution composition upon the carbon dioxide chemisorption on a platinized platinum electrode. *Sov. Electrochem.* **1968**, *4*, 1374–1378.
36. Vasina, S.Y.; Petry, O.A. Perchlorate anions adsorption on platinum and rhodium electrodes. *Sov. Electrochem.* **1970**, *6*, 242–246.
37. Bunkin, N.F.; Yurchenko, S.O.; Suyazov, N.V.; Shkirin, A.V. Structure of the nanobubble clusters of dissolved air in liquid media. *J. Biol. Phys.* **2012**, *38*, 121–152. [[CrossRef](#)]
38. Heinze, J. Ultramicroelectrodes in Electrochemistry. *Angew. Chem. Int. Ed. Engl.* **1993**, *32*, 1268–1288. [[CrossRef](#)]

39. Wilhelm, E.; Battino, R.; Wilcock, R.J. Low-Pressure Solubility of Gases in Liquid Water. *Chemical. Rev.* **1977**, *77*, 219–262. [[CrossRef](#)]
40. Palmer, D.A.; Eldik, R.V. The chemistry of metal carbonato and carbon dioxide complexes. *Chem. Rev.* **1983**, *83*, 651–731. [[CrossRef](#)]
41. Becke, A.D. Density-functional thermochemistry. III. The role of exact exchange. *J. Chem. Phys.* **1993**, *98*, 5648–5652. [[CrossRef](#)]
42. Lee, C.; Yang, W.; Parr, R. Development of the Colle-Salvetti Correlation-Energy Formula into a Functional of the Electron Density. *J. Phys. Rev. B* **1988**, *37*, 785–789. [[CrossRef](#)] [[PubMed](#)]
43. Vosko, S.H.; Wilk, L.; Nusair, M. Accurate spin-dependent electron liquid correlation energies for local spin density calculations: A critical analysis. *Can. J. Phys.* **1980**, *58*, 1200–1211. [[CrossRef](#)]
44. Stevens, W.J.; Krauss, M.; Basch, H.; Jasien, P.G. Relativistic compact effective potentials and efficient, shared-exponent basis sets for the third-, fourth-, and fifth-row atoms. *Can. J. Chem.* **1992**, *70*, 612–630. [[CrossRef](#)]
45. Schmidt, M.W.; Baldridge, K.K.; Boatz, J.A.; Elbert, S.T.; Gordon, M.S.; Jensen, J.J.; Koseki, S.; Matsunaga, K.A.; Nguyen, S.S.; Windus, T.L.; et al. General atomic and molecular electronic structure system. *J. Comput. Chem.* **1993**, *14*, 1347–1363. [[CrossRef](#)]
46. Granovsky, A.A. Firefly, Version 8. Available online: [wwwhttp://classic.chem.msu.su/gran/firefly/index.html](http://classic.chem.msu.su/gran/firefly/index.html) (accessed on 31 December 2020).
47. Glendening, E.D.; Badenhoop, J.K.; Reed, A.E.; Carpenter, J.E.; Bohmann, J.A.; Morales, C.M.; Weinhold, F. *NBO 5.9*; Theoretical Chemistry Institute, University of Wisconsin: Madison, WI, USA, 2012.
48. Rodes, A.; Pastor, E.; Iwasita, T. Structural effects on CO₂ reduction at Pt single-crystal electrodes. Part 2. Pt(111) and vicinal surfaces in the [011] zone. *J. Electroanal. Chem.* **1994**, *373*, 167–175. [[CrossRef](#)]
49. Iwasita, T.; Nart, F.C.; Lopez, B.; Vielstich, W. On the study of adsorbed species at platinum from methanol, formic acid and reduced carbon dioxide via in situ ft-ir spectroscopy. *Electrochim. Acta* **1992**, *37*, 2361–2367. [[CrossRef](#)]
50. Markovic, N.M.; Ross, P.N. Surface science studies of model fuel cell electrocatalysts. *Surf. Sci. Rep.* **2002**, *45*, 117–229. [[CrossRef](#)]
51. Mayrhofer, K.J.J.; Arenz, M.; Blizanac, B.; Stamenkovich, V.; Ross, P.N.; Markovic, N.M. CO surface electrochemistry on Pt-nanoparticles: A selective review. *Electrochim. Acta* **2005**, *50*, 5144–5154. [[CrossRef](#)]
52. Cuesta, A. The oxidation of adsorbed CO on Pt(100) electrodes in the pre-peak region. *Electrocatalysis* **2010**, *1*, 7–18. [[CrossRef](#)]
53. Cuesta, A. Electrooxidation of C1 organic molecules on Pt electrodes. *Curr. Opin. Electrochem.* **2017**, *4*, 32–38. [[CrossRef](#)]
54. Brimaud, S.; Pronier, S.; Contanceau, C.; Leger, J.M. New findings on CO electrooxidation at platinum nanoparticle surfaces. *Electrochem. Commun.* **2008**, *10*, 1703–1707. [[CrossRef](#)]
55. Urchada, P.; Baranton, S.; Coutanceau, C.; Jerkiewicz, G. Electro-oxidation of CO_{chem} on Pt Nanosurfaces: Solution of the Peak Multiplicity Puzzle. *Langmuir* **2012**, *28*, 3658–3663. [[CrossRef](#)] [[PubMed](#)]
56. Wang, H.; Jusus, Z.; Behm, R.J.; Abruna, H.D. New Insights into the Mechanism and Kinetics of Adsorbed CO Electrooxidation on Platinum: Online Mass Spectrometry and Kinetic Monte Carlo Simulation Studies. *J. Phys. Chem. C* **2012**, *116*, 11040–11053. [[CrossRef](#)]
57. Wang, H.; Abruna, H.D. Origin of Multi-peaks in the Potentiodynamic Oxidation of CO Adlayers on Pt and Ru-modified Pt Electrodes. *J. Phys. Chem. Lett.* **2015**, *6*, 1899–1906. [[CrossRef](#)]
58. Farias, M.J.S.; Buso-Rogero, C.; Vidal-Iglesias, F.J.; Solla-Gullon, J.; Camara, G.A.; Feliu, J.M. Mobility and Oxidation of Adsorbed CO on Shape-Controlled Pt Nanoparticles in Acidic Medium. *Langmuir* **2017**, *33*, 865–871. [[CrossRef](#)]
59. Arevalo, M.C.; Gomis-Bas, C.; Hahn, F.; Beden, B.; Arevalo, A.; Arvia, A.J. A contribution to the mechanism of “reduced” CO₂ adsorbates electro-oxidation from combined spectroelectrochemical and voltammetric data. *Electrochim. Acta* **1994**, *39*, 793–799. [[CrossRef](#)]
60. Tokarz, W.; Siwek, H.; Piela, P.; Czerwiński, A. Electro-oxidation of methanol on Pt-Rh alloys. *Electrochim. Acta* **2007**, *52*, 5565–5573. [[CrossRef](#)]
61. Łukaszewski, M.; Czerwiński, A. Comparative EQCM study on electrooxidation of carbon oxides adsorption products on noble metals and their alloys. Polycrystalline Pd-based systems. *J. Electroanal. Chem.* **2007**, *606*, 117–133.
62. Behm, R.J.; Thiel, P.A.; Norton, P.R.; Ertl, G. The interaction of CO and Pt(100). I. Mechanism of adsorption and Pt phase transition. *J. Chem. Phys.* **1983**, *78*, 7437–7447. [[CrossRef](#)]
63. Yang, S.; Noguchi, H.; Uosaki, K. Broader energy distribution of CO adsorbed at polycrystalline Pt electrode in comparison with that at Pt(111) electrode in H₂SO₄ solution confirmed by potential dependent IR/visible double resonance sum frequency generation spectroscopy. *Electrochim. Acta* **2017**, *235*, 280–286. [[CrossRef](#)]
64. Lykianicheva, V.I.; Bagotskii, V.S. Oxygen adsorption on smooth degassed platinum in electrolyte solutions. *Dokl. Akad. Nauk SSSR* **1964**, *155*, 160–163.
65. Tikhomirova, V.I.; Lukyanychev, V.I.; Bagotsky, V.S. Oxygen-hydrogen peroxide equilibrium on outgassed platinum in the presence of oxygen traces. *Sov. Electrochem.* **1965**, *1*, 645–650.
66. Johnson, M. *Correlations of Cycles in Weather, Solar Activity, Geomagnetic Values and Planetary Configurations*; Phillips and Van Orden: San Francisco, CA, USA, 1944; p. 149.
67. Martins, M.E. Electrochemical behaviour of carbon dioxide on platinum and rhodium. *J. Argent. Chem. Soc.* **2005**, *93*, 143–153.
68. Baruzzi, A.M.; Leiva, E.P.M.; Giordano, M.C. The influence of solution composition on the kinetics of “reduced” CO₂ electrooxidation at polycrystalline platinum. *J. Electroanal. Chem. Interfacial Electrochem.* **1985**, *189*, 257–269. [[CrossRef](#)]

69. Baruzzi, A.M.; Leiva, E.P.M.; Giordano, M.C. Complex kinetic behaviour of “reduced” CO₂ electro-oxidation at Pt electrodes. *J. Electroanal. Chem. Interfacial Electrochem.* **1983**, *158*, 103–114.
70. Bagotskii, V.S.; Nekrasov, L.N.; Shumilova, N.A. Electrochemical Reduction of Oxygen. *Russ. Chem. Rev. (Uspekhi Khimii)* **1965**, *34*, 717–730. [[CrossRef](#)]
71. Noel, J.-M.; Latus, A.; Lagrost, C.; Volanschi, E.; Hapiot, P. Evidence for OH Radical Production during Electrocatalysis of Oxygen Reduction on Pt Surfaces: Consequences and Application. *J. Am. Chem. Soc.* **2012**, *134*, 2835–2841. [[CrossRef](#)]
72. Chen, J.; Fang, L.; Luo, S.; Liu, Y.; Chen, S. Electrocatalytic O₂ Reduction on Pt: Multiple Roles of Oxygenated Adsorbates, Nature of Active Sites and Origin of Overpotential. *J. Phys. Chem. C* **2017**, *121*, 6209–6217. [[CrossRef](#)]
73. Gomez-Marín, A.M.; Feliu, J.M.; Ticianelli, E. Oxygen Reduction on Platinum Surfaces in Acid Media: Experimental Evidence of a CECE/DISP Initial Reaction Path. *ACS Catal.* **2019**, *9*, 2238–2251.
74. Nørskov, J.K.; Rossmeisl, J.; Logadottir, A.; Lindqvist, L.; Kitchin, J.R.; Bligaard, T.; Jónsson, H. Origin of the Overpotential for Oxygen Reduction at a Fuel-Cell Cathode. *J. Phys. Chem. B* **2004**, *108*, 17886–17892. [[CrossRef](#)]
75. Damjanovic, A.; Brusic, V. Electrode kinetics of oxygen reduction on oxide-free platinum electrodes. *Electrochim. Acta* **1967**, *12*, 615–628. [[CrossRef](#)]
76. Jinnouchi, R.; Kodama, K.; Hatanaka, T.; Morimoto, Y. First principles based mean field model for oxygen reduction reaction. *Phys. Chem. Chem. Phys.* **2011**, *13*, 21070–21083. [[CrossRef](#)]
77. Hansen, H.A.; Viswanathan, V.; Nørskov, J.K. Unifying Kinetic and Thermodynamic Analysis of 2 e⁻ and 4 e⁻ Reduction of Oxygen on Metal Surfaces. *J. Phys. Chem. C* **2014**, *118*, 6706–6718. [[CrossRef](#)]
78. Staszak-Jirkovský, J.; Ahlberg, E.; Panas, I.; Schiffrin, D.J. The bifurcation point of the oxygen reduction reaction on Au–Pd nanoalloys. *Faraday Discuss.* **2016**, *188*, 257–278. [[CrossRef](#)]
79. Gómez-Marín, A.M.; Rizo, R.; Feliu, J.M. Oxygen reduction reaction at Pt single crystals: A critical overview. *Catal. Sci. Technol.* **2014**, *4*, 1685–1698. [[CrossRef](#)]
80. Ruvinskiy, P.S.; Bonnefont, A.; Pham-Huu, C.; Savinova, E.R. Using Ordered Carbon Nanomaterials for Shedding Light on the Mechanism of the Cathodic Oxygen Reduction Reaction. *Langmuir* **2011**, *27*, 9018–9027. [[CrossRef](#)]
81. Gomez-Marín, A.M.; Feliu, J.M. New Insights into the Oxygen Reduction Reaction Mechanism on Pt(111): A Detailed Electrochemical Study. *Chemsuschem* **2013**, *6*, 1091–1100. [[CrossRef](#)]
82. Schumb, W.C.; Satterfield, C.N.; Wentworth, R.L. *Hydrogen Peroxide*; Reinold Publishing Corp.: New York, NY, USA; Chapman & Nall, Ltd.: London, UK, 1956; p. 579.
83. Schmidt, V.M.; Rodriguez, J.L.; Pastor, E. The Influence of H₂O₂ on the Adsorption and Oxidation of CO on Pt Electrodes in Sulfuric Acid Solution. *J. Electrochem. Soc.* **2001**, *148*, A293–A298. [[CrossRef](#)]
84. Martinez, S.; Zinola, F.; Planes, G.; Guillén-Villafuerte, O.; Rodriguez, J.L.; Pastor, E. The influence of hydrogen peroxide on carbon monoxide electrooxidation at Pt/C and Pt:Ru/C electrodes. *J. Solid State Electrochem.* **2007**, *11*, 1521–1529. [[CrossRef](#)]
85. Briega-Martos, V.; Herrero, E.; Feliu, J.M. The inhibition of hydrogen peroxide reduction at low potentials on Pt(111): Hydrogen adsorption or interfacial charge? *Electrochem. Commun.* **2017**, *85*, 32–35. [[CrossRef](#)]
86. Takahashi, M.; Chiba, K.; Li, P. Free-Radical Generation from Collapsing Microbubbles in the Absence of a Dynamic Stimulus. *J. Phys. Chem. B* **2007**, *111*, 1343–1347. [[CrossRef](#)] [[PubMed](#)]
87. Gudkov, S.; Bruskov, V.; Astashev, M.; Chernikov, A.; Yaguzhinsky, L.; Zakharov, S. Oxygen Dependent Auto-Oscillations of Water Luminescence Triggered by the 1264 nm Radiation. *J. Phys. Chem. B* **2011**, *115*, 7693–7698. [[CrossRef](#)] [[PubMed](#)]
88. Bunkin, N.F.; Shkirin, A.V.; Ignatiev, P.S.; Chaikov, L.L.; Burkhanov, I.S.; Starosvetskij, A.V. Nanobubble clusters of dissolve gas in aqueous solutions of electrolyte. I. Experimental proof. *J. Chem. Phys.* **2012**, *137*, 054706-1–054706-10.
89. Bunkin, N.F.; Suyazov, N.V.; Shkirin, A.V.; Ignatiev, P.S.; Indukaev, K.V. Nanoscale structure of dissolved air bubbles in water as studied by measuring the elements of the scattering matrix. *J. Chem. Phys.* **2009**, *130*, 134308-1–134308-12. [[CrossRef](#)]
90. Ushikubo, F.Y.; Enari, M.; Furukawa, T.; Nakagawa, R.; Makino, Y.; Kawagoe, Y.; Oshita, S. Zeta-potential of micro-and/or nano-bubbles in water formed by certain types of gases. *Ifac Proc. Vol.* **2010**, *43*, 283–288. [[CrossRef](#)]
91. Buchachenko, A. *Magneto-Biology and Medicine*; Nova Science Publishers: New York, NY, USA, 2014; p. 225.
92. Roberts, J.G.; Voinov, M.A.; Schmidt, A.C.; Smirnova, T.I.; Sombers, L.A. The Hydroxyl Radical is a Critical Intermediate in the Voltammetric Detection of Hydrogen Peroxide. *J. Am. Chem. Soc.* **2016**, *138*, 2516–2519. [[CrossRef](#)]
93. Villegas, I.; Weaver, M.J. Carbon monoxide adlayer structures on platinum (111) electrodes: A synergy between insitu scanning tunneling microscopy and infrared spectroscopy. *J. Chem. Phys.* **1994**, *101*, 1648–1660. [[CrossRef](#)]
94. Inukai, J.; Tryk, D.A.; Abe, T.; Wakisaka, M.; Uchida, H.; Watanabe, M. Direct STM Elucidation of the Effects of Atomic-Level Structure on Pt(111) Electrodes for Dissolved CO Oxidation. *J. Am. Chem. Soc.* **2013**, *135*, 1476–1490. [[CrossRef](#)] [[PubMed](#)]
95. Podlovchenko, B.I.; Gladysheva, T.D.; Kolyadko, E.A. Experimental check-up of the relationship between transients of current and open circuit potential for strong adsorption of neutral species and ions on a hydrogen electrode. *J. Electroanal. Chem.* **2003**, *552*, 85–96. [[CrossRef](#)]
96. Petrii, O.A. Zero Charge Potentials of Platinum Metals and Electron Work Functions (Review). *Russ. J. Electrochem.* **2013**, *49*, 401–422. [[CrossRef](#)]
97. Martínez-Hincapié, R.; Berná, A.; Rodes, A.; Climent, V.; Feliu, J.M. Surface Acid–Base Properties of Anion-Adsorbed Species at Pt(111) Electrode Surfaces in Contact with CO₂-Containing Perchloric Acid Solutions. *J. Phys. Chem. C* **2016**, *120*, 16191–16199. [[CrossRef](#)]

98. Huber, K.P.; Herzberg, G. *Molecular Spectra and Molecule Structure. IV. Constants of Diatomic Molecules*; Van Nostrand Reinhold Comp.: New York, NY, USA; Cincinnati, OH, USA; Atlanta, GA, USA; Dallas, TX, USA; San Francisco, CA, USA; London, UK; Toronto, ON, Canada; Melbourne, Australia, 1979.
99. Thiel, P.A.; Behm, R.J.; Norton, P.R.; Ertl, G. The interaction of CO and Pt(100). II. Energetic and kinetic parameters. *J. Chem. Phys.* **1983**, *78*, 7448–7458. [[CrossRef](#)]
100. Noguchi, H.; Okada, T.; Uosaki, K. SFG study on potential-dependent structure of water at Pt electrode/electrolyte solution interface. *Electrochim. Acta* **2008**, *53*, 6841–6844. [[CrossRef](#)]
101. Vassilyev, Y.B.; Khazova, O.A.; Nikolaeva, N.N. Kinetics and mechanism of glucose electrooxidation on different electrode-catalysts. Part. I. Adsorption and oxidation on platinum. *J. Electroanal. Chem. Interfacial Electrochem.* **1985**, *196*, 105–125. [[CrossRef](#)]
102. Vassilyev, Y.B.; Khazova, O.A.; Nikolaeva, N.N. Kinetics and mechanism of glucose electrooxidation on different electrode-catalysts part II. effect of the nature of the electrode and the electrooxidation mechanism. *J. Electroanal. Chem. Interfacial Electrochem.* **1985**, *196*, 127–144. [[CrossRef](#)]
103. Lavrik, N.L.; Bazhin, N.M. On the Impossibility of OH Radical Formation from the Hydroxyl Ion in Water. *Biophysics* **2011**, *56*, 535–536. [[CrossRef](#)]
104. Solans-Monfort, X.; Branchadell, V.; Sodupe, M.; Sierka, M.; Sauer, J. Electron hole formation in acidic zeolite catalysts. *J. Chem. Phys.* **2004**, *121*, 6034–6040. [[CrossRef](#)]
105. Chen, H.; Handoko, A.D.; Xiao, J.; Feng, X.; Fan, Y.; Wang, T.; Legut, D.; Seh, Z.W.; Zhang, Q. Catalytic effect on CO₂ electroreduction by hydroxyl terminated two-dimensional MXenes. *ACS Appl. Mater. Interfaces* **2019**, *11*, 36571–36579. [[CrossRef](#)] [[PubMed](#)]
106. Handoko, A.D.; Khoo, K.H.; Tan, T.L.; Jin, H.; Seh, Z.W. Establishing new scaling relations on two-dimensional MXenes for CO₂ electroreduction. *J. Mater. Chem. A* **2018**, *6*, 21885–21890. [[CrossRef](#)]
107. Handoko, A.D.; Wei, F.; Yeo, B.S.; Seh, Z.W. Understanding heterogeneous electrocatalytic carbon dioxide reduction through operando techniques. *Nat. Catal.* **2018**, *1*, 922–934. [[CrossRef](#)]
108. Handoko, A.D.; Steinmann, S.N.; Seh, Z.W. Theory-guided materials design: Two-dimensional MXenes in electro- and photocatalysis. *Nanoscale Horiz.* **2019**, *4*, 809–827. [[CrossRef](#)]